A general mass transfer equation for gas-evolving electrodes

Haverkort, J. W.

DOI
10.1016/j.ijhydene.2024.06.010

Publication date
2024

Document Version
Final published version

Published in
International Journal of Hydrogen Energy

International Journal of Hydrogen Energy 74 (2024) 283–296

Contents lists available at ScienceDirect

International Journal of Hydrogen Energy

journal homepage: www.elsevier.com/locate/he

A general mass transfer equation for gas-evolving electrodes

J.W. Haverkort

Delft University of Technology, Process & Energy Department, Leeghwaterstraat 39, Delft, 2628 CB Delft, The Netherlands

ARTICLE INFO

Keywords:
Mass transfer
Gas evolution
Natural convection
Micromixing
Electrocapillarity
Marangoni flows

ABSTRACT

Poor mass transport to or from vertical gas-evolving electrodes can adversely impact energy efficiency and product purity in the production of hydrogen, chlorine, and various metals. A proper description that combines natural convection with micromixing of growing, coalescing, and departing bubbles is presently lacking. This work develops a simple, physically sound analytical model that includes the influence of bubble size, flow regime, and bubble surface coverage. By comprehensively reviewing mass transfer measurements from the water electrolysis literature, we observe that the surface coverage of oxygen bubbles increases much more strongly with increasing current density than an often-used square root scaling predicts. Strong differences are observed in the degree of micromixing of hydrogen and oxygen bubbles in alkaline and acidic electrolytes. These varied results can all be explained by a combination of electrocapillarity, and coalescence induced by either a high surface coverage or Marangoni flows.

1. Introduction

Important industrial processes like water electrolysis, the chlor-alkali process, and the production of aluminium involve vertical electrodes from which gas bubbles emanate. Gaseous reaction products are created in dissolved form, which supersaturate the solution and subsequently produce bubbles. These bubbles provide inexpensive stirring caused by their growth, coalescence, and detachment from the electrodes. This will further be referred to as *micromixing*. In addition, rising bubbles create natural convection flows, further increasing mass transport. We consider here the challenge of how to model the combination of micromixing and the *macromixing* due to flows caused by natural or forced convection.

Comprehensive reviews on gas-evolving electrodes are provided in Refs. [1–4]. Here, we only give a concise historical account of a limited number of important works in the area of mass transfer. Various works used fast redox couples to measured, as a function of reactant concentration c, the average reactant flux N [mol/m^2/s]: the amount of reactant converted per unit time per electrode area. When the reaction is sufficiently fast, the reactant concentration at the electrode vanishes and the mass transfer coefficient between the bulk and the electrode surface is obtained as $k = N/c$ [5]. Already mid-way through the last century, it was found that micromixing mass transfer coefficients approximately scale with current density j as $k \propto j^{1/2}$, [6]. This was confirmed by various other works, see for example Ref. [7] and Table 1. This was initially explained [8,9] by the transient diffusion flux causing replenishment after the departure of a bubble, which has a square-root dependence on time, similar to classical surface renewal or penetration theory [10]. Also, bubble growth [7], rising bubbles sweeping the electrode [11], bubbles coalescing [12] and subsequently jumping from the electrode [11] give rise to a similar dependence. Ref. [2] shows that the analysis of Ref. [13], scrutinised in Ref. [14], also essentially gives the same result. We will use the term micromixing for all these bubble phenomena local to the electrode that increase the mass transfer. The mass transfer coefficient has sometimes also been found to increase with current density to a higher power than 1/2 as shown in Table 1. This has been attributed to enhanced micromixing due to coalescence [12,15], in agreement with an observed increase in bubble size. In alkaline electrolytes, coalescence was found to play a significant role already at quite low current densities of about 30 mA/cm^2 for oxygen bubbles [12,16] but only around 1.5 A/cm^2 for hydrogen bubbles [12]. Coalescence can give rise to very high liquid velocities near the electrode surface of several meters per second [17], explaining its effectiveness in increasing mass transport [18].

Natural convection flows can arise in electrochemical processes due to solutal effects [19–23] and temperature [24]. However, for gas-evolving electrodes, flow is usually dominated by the buoyancy of gas bubbles. In keeping with the literature, we will refer to the flows induced by bubbles also as natural convection. Ref. [25] used an analogy with thermal natural convection to describe heat transfer in boiling. This same analogy has been used by, e.g. Refs. [26,27] for turbulent and laminar flow, respectively, both assuming a constant wall gas fraction. We will here extend these analyses to include the

E-mail address: J.W.Haverkort@tudelft.nl.
URL: https://jwhaverkort.weblog.tudelft.nl.

https://doi.org/10.1016/j.ijhydene.2024.06.010
Received 7 March 2024; Received in revised form 28 May 2024; Accepted 1 June 2024
Available online 14 June 2024

Nomenclature

a	Relative area impacted by micromixing [−]
$\mathcal{V}_m$	Gas molar volume RT/p
a_{ref}	Reference a defined by Eq. (3) [−]
θ	Bubble surface coverage
A	Electrode area [m^2]
c	Concentration [mol/m^3]
c_p	Heat capacity [J/kg/K]
D	Diffusivity [m^2/s]
d	Bubble diameter [m]
f_g	Gas evolution efficiency [−]
h	Height of a vertical electrode [m]
j	Current density [A/m^2]
k	Electrode-bulk mass transfer coefficient $N/\Delta c$ [m/s]
N	Flux of gas [mol/m^2/s]
n	Number of electrons per gas molecule [−]
p	Power in $k \propto j^p$, or $\partial \ln k/\partial \ln j$ [−]
t	Time [s]
U_g	Volumetric electrode gas flux [m/s]
z	Vertical coordinate [m]

Constants

F	Faraday's constant 96485.332... [C/mol]
R	Gas constant 8.31446... [J/mol/K]

Greek variables

γ	Surface tension [N/m]
ν	Liquid kinematic viscosity [m^2/s]
ρ	Liquid density [kg/m^3]
ϵ	Gas fraction

Subscripts and other notation

μ	micromixing
’	local value near a bubble
b	bubble
d	discharge
f	flow, free and/or forced
g	gas
l	liquid

more relevant boundary condition of constant gas flux and the effect of bubble size on the dispersion coefficient.

Simply adding the contributions of micromixing and natural convection [28], as is often done, has been scrutinised in further works [11,29,30]. Ref. [31] concluded that "*the proper addition rule to be employed remains undecided*". The effects of bubble size, surface coverage, and the polarisation of electrode and electrolyte can have large effects that most relations do not take into account. An exception is the comprehensive model introduced in [11,32,33], which, however, has only been formulated and tested for forced convection. Unfortunately, at the end of the 1980s, a period of intensive research into the effect of gas evolution on mass transfer came to a somewhat abrupt halt.

Recently, experiments on micro-electrodes and simulations have improved our understanding of bubble growth [34–37], coalescence [38,39], and release [40–42][40,41]. For example, droplets [43] or a bubble micro-carpet [39,44,45][44,45] were shown to sometimes exist below large bubbles on micro-electrodes. The relevance of electrical forces is still under debate [44,46], but the importance of solutal Marangoni flows is becoming evident [45,47].

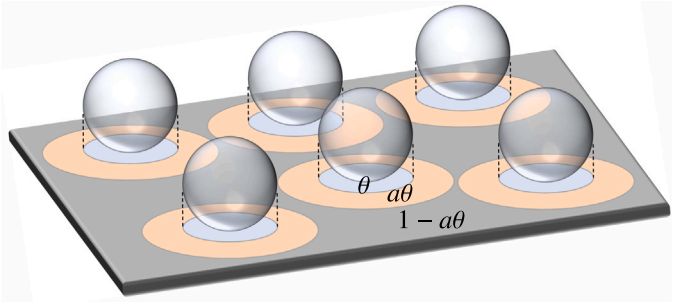

Fig. 1. The bubble surface coverage θ is the fractional projected electrode area below bubbles. The product $a\theta$ gives the fractional electrode area effectively impacted by micromixing.

In modern devices and reactors, the flat planar electrodes used in most past experiments are often replaced by meshes, expanded metals, or otherwise structured electrodes. However, because the mass transfer boundary layer is usually much thinner than the electrode features, their surface can still be considered to be flat locally. Therefore, previous results on planar electrodes continue to hold relevance for more complex electrode shapes. We do note that in case the local current density varies in space, the relationships derived in this work have to applied locally and averaged in some appropriate manner, for example through computational simulations.

The limiting cases of micro- and macro-mixing sometimes work reasonably well in explaining experimental data. However, more often than not, the data is more complicated. For example, the bubble size can vary between experimental conditions, significantly influencing mass transfer [14]. Therefore, a more general physical model is required that takes into account the effect of bubble parameters like diameter, surface coverage, and coalescence tendency.

The motivation for this work is to understand the influence of bubble size, coverage, current density, and type of electrode and electrolyte on mass transfer. The objective and novelty of this work is a mathematical relation that describes the variation in experiments in a physically consistent and compact way, including the effect of both natural convection flows and bubble micromixing.

2. Micromixing, e.g. for H_2 in H_2SO_4

Fig. 1 introduces the *bubble surface coverage* θ as the ratio of the projected area below the adhering bubbles and the total electrode area A. Therefore, it represents the fraction of the electrode 'in the shadow' of the adhering bubbles. In the surface renewal model of micromixing, it is assumed that departing bubbles thoroughly mix the fluid in the entire boundary layer over an area $a\theta A$. The dimensionless impacted-area parameter a thus signifies the electrode area impacted by micromixing relative to the area that bubbles cover. Fig. 1 shows an example in which $a > 1$, so that the area impacted by micromixing is larger than the projected bubble area, but it might also be smaller so that $a < 1$. In this impacted area, the concentration is assumed to attain its bulk value after each bubble leaves, and subsequently, its boundary layer thickness increases as described by the one-dimensional diffusion equation, see Fig. 6. On vertical electrodes, the value of a may also be much larger than 1 because, they may remain close to the electrode while rising and mix a region much larger than just their shadow [11,31]. The resulting time- and mass-averaged mass transfer coefficient k is derived in Appendix A. For a constant bubble diameter d, Eq. (A.2) gives the micromixing mass transfer coefficient as

$$k_\mu = a\sqrt{\frac{6\theta D U_g}{\pi d}}. \tag{1}$$

Table 1
Various experimental results (an update of Ref. [30] which updated Refs. [2], [48] and [49]) grouped by the power $p = \partial \ln k / \partial \ln j$ with which the mass transfer coefficient k scales with the current density j. As alkaline electrolytes both KOH and NaOH are used and as acidic electrolyte only H_2SO_4 was used. Low values $p < 0.4$ are found in alkaline electrolytes for H_2-evolving electrodes and for O_2-evolving electrodes at low to moderate current densities. Large values $p > 0.65$ have been attributed to coalescence and occur mostly at very high current densities.

$k \propto j^p$	Conditions	First author and year (*horizontal electrodes*, new additions)
$p < 0.4$	H_2 alkaline	Vondrak '70 [50], Fouad '72 [51] *Fouad '73* [52], Janssen '73 [15], Janssen '78 [14], *Janssen '79* [53] ($j < 10^4$ A/m^2)
	O_2 alkaline	Janssen '70 [54], Fouad '72 [51] ($j < 500$ A/m^2), Janssen '73 [15] ($j \lesssim 200$ A/m^2), *Janssen '79* ($j < 200$ A/m^2) [53]
$0.4 \gtrsim p \lesssim 0.65$	H_2 alkaline	*Green '59* [55], *Janssen '79* [12] (both $j \gtrsim 10^4$ A/m^2), Hiraoka '86 [56]
	O_2 alkaline	Hiraoka '86 [56], *Janssen '73* [15]
	H_2 acidic	*Kind '75* [57], Janssen '70 [54], Roald '51 [6], Fukunaka '89[58], Venczel '61 [8], Alkire '79 (j>800 A/m^2) [59] , *Janssen '73* [15]
	O_2 acidic	Janssen'70 [54], Beck '69 [28], Ibl '71, Chen '88 [60], *Janssen '73* [15]
$0.65 < p < 1$	O_2 alkaline	*Janssen '78* [14], *Janssen '73* [15], *Janssen '79* [12] (all $j \gtrsim 300$ A/m^2)
	O_2 acidic	*Kind '75* [57] ($j \gtrsim 10^4$ A/m^2), Ibl '71 [48] ($j \gtrsim 3 \cdot 10^3$ A/m^2)
	H_2 acidic	*Kind '75* [57] ($j \gtrsim 3 \cdot 10^5$ A/m^2)

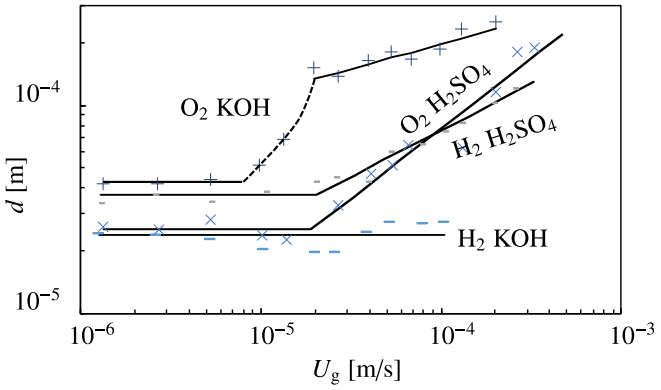

Fig. 2. The volume-averaged bubble diameter ($(\Sigma_{i=1}^{n} d_i^3/n)^{1/3}$) measured from enlarged images 0.2 mm above a horizontal platinum electrode that was 1.12 cm in diameter in 1 M KOH or H_2SO_4, from Ref. [63].

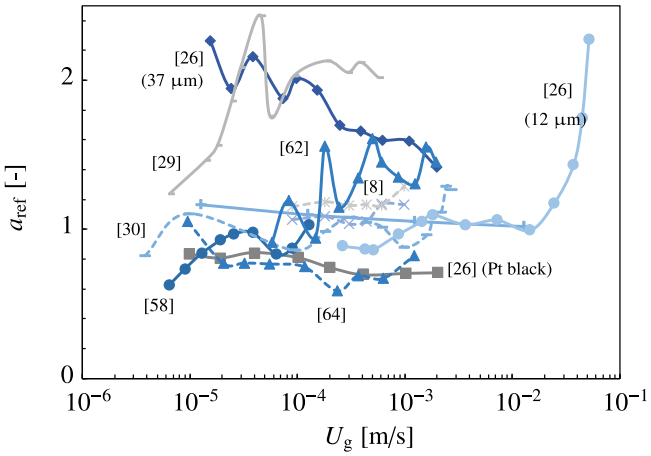

Fig. 3. For hydrogen bubbles in sulphuric acid (H_2SO_4) the parameter a_{ref}, defined by Eq. (3), does not depend on gas flux $U_g = j\mathcal{V}_m/2F$ for most of the data obtained from the literature. Solid and dashed lines concern experiments with horizontal and vertical electrodes, respectively. The line colour and marker type only differ to be able to distinguish the different sources better. For Ref. [57] the grain size of the sanding paper used for treating the platinum electrodes is indicated.

Here U_g [m^3/m^2/s] or [m/s] is the volumetric gas flux, or superficial gas velocity, through the electrode surface. Therefore, it can be written as

$$U_g = f_g \frac{j\mathcal{V}_m}{nF}. \tag{2}$$

Here j [A/m^2] is the current density, $\mathcal{V}_m$ [m^3/mol] is the gas molar volume, F [C/mol] is Faraday's constant, n [−] represents the number of gas molecules produced per electron, and the gas-evolution efficiency f_g [−] denotes the fraction of the produced gas that enters the gas bubbles before they leave the surface; the remaining fraction $1 - f_g$ leaves the adherence region as dissolved gas [61].

When $a\sqrt{f_g\theta/d}$ is approximately independent of current density, Eq. (1) predicts a mass transfer coefficient that increases with the square root of current density. Usually, $f_g\theta/d$ cannot be obtained from reported experimental results so a cannot be determined. Therefore, we introduce a new parameter:

$$a_{ref} \equiv \frac{k}{\sqrt{\frac{6D}{\pi}\frac{j\mathcal{V}_m}{nF}\left(\frac{f_g\theta}{d}\right)_{ref}}} \xrightarrow{k=k_\mu} a\sqrt{\frac{f_g\theta}{d}\left(\frac{d}{f_g\theta}\right)_{ref}} \tag{3}$$

where we take $d_{ref}/f_g\theta_{ref} = 200$ μm.[1]

Fig. 3 shows an overview of all relevant measurements we found in the open literature for hydrogen bubbles in sulphuric acid, H_2SO_4. All graphs in this work with U_g used Eq. (2) with $f_g = 1$ to convert from reported current densities. This allows hydrogen $n = 2$ and oxygen $n = 4$ results to be compared on a more equal basis.

As is expected for micromixing, the parameter a_{ref} is of the order one and for most experiments hardly depends on current density. By Eq. (3), a constant value of a_{ref} implies a mass transfer coefficient that increases proportional to j^p with $p = 1/2$. We note that Fig. 3 shows no obvious differences between horizontal and vertical configurations. This demonstrates that electrode orientation at most only subtly influences micromixing mass transfer.

In Table 1 we provide a more or less comprehensive overview of all relevant experimental mass transfer investigations in H_2SO_4, NaOH, and KOH. Most results have a value of $p \approx 0.5$ as expected for dominant micromixing. However, oxygen-evolution shows substantially higher values for p above $\gtrsim$ 300 A/m^2 in alkaline electrolytes. In acidic electrolytes this happens at much higher current densities $\gtrsim 3 \cdot 10^3$ A/m^2. Likely, this enhancement in mass transfer can be attributed to coalescence events which are particularly effective at stirring the fluid.

We also see several experimental results with a value of p substantially below 0.5, for all results with hydrogen bubbles in alkaline electrolytes and for oxygen at low current densities. To explain this, we will now consider the effect of natural convection flows on mass transfer.

[1] This corresponds to, for example $d_{ref} = 50$ μm and $\theta_{ref} = 0.25$ or $d_{ref} = 100$ μm and $\theta_{ref} = 0.5$, representative for high current densities, see Fig. 2 and Section 4.2, so $a_{ref} \sim a$. With decreasing current density, both the surface coverage, see Section 4.2, and gas evolution efficiency [33,62] will tend to zero, unlike the bubble diameter, so that for low current densities $a_{ref} \ll a$.

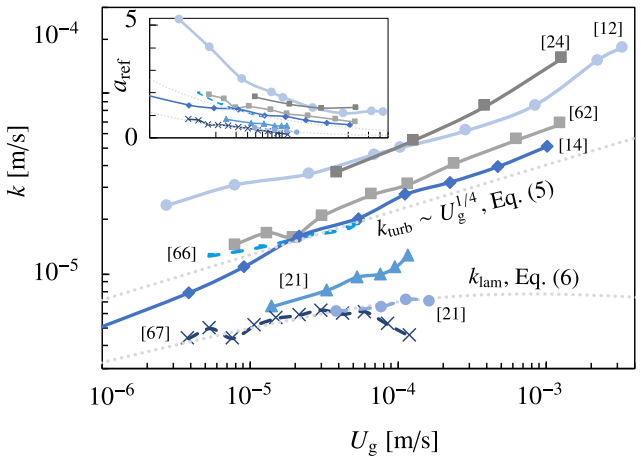

Fig. 4. Literature data on the mass transfer coefficient for hydrogen evolution in alkaline electrolytes (KOH or NaOH). The solid lines represent horizontal electrodes while the dashed lines are vertical electrodes. The inset shows a_{ref}, defined in Eq. (3), on the same horizontal scale and range as the main graph. The turbulent relation of Eq. (5) uses $D = 7.9 \cdot 10^{-10}$ m^2/s relevant for 1 M KOH [63] and the vertical laminar relation of Eq. (6) uses $D = 4.75 \cdot 10^{-10}$ m^2/s relevant for 2 M NaOH [19]. Both relations describe several literature results quite well. From Ref. [65] we selected the data for 50 cm height and a 4 cm gap. Refs. [12,55,63] used very small electrodes of less than 12 mm diameter, so that edge effects likely increased the mass transfer. The horizontal data of Ref. [52] used a thin rod counter electrode, resulting in a strongly inhomogeneous current distribution, making these results less reliable. An exceptionally large scatter in the data of Ref. [66], because of which we applied a moving average, casts some doubts on the accuracy.

3. Natural convection, e.g. for H_2 in KOH

Rising bubbles experience random sideways deviations from their upwards motion due to interactions with other bubbles, by analogy to the flow through a porous medium this is called hydrodynamic dispersion. From experiments with solid particles [64], the bubble dispersion coefficient is given by Eq. (4) as

$$D_b = \frac{g d^3}{36\nu} \tag{4}$$

For higher gas fractions, flow shear can increase the dispersion, but often turbulence sets in and turbulent dispersion becomes dominant. With advection and diffusion being the dominant transfer mechanism for bubbles, we can use an analogy with thermal natural convection for which various heat transfer coefficient expressions have been developed.

Under turbulent conditions we find Eq. (B.7) for both upwards facing and vertical electrodes, which upon inserting Eq. (4) reads,[2]

$$k_{turb} = 0.27 \left(\frac{g U_g}{\nu D_b^{2/3}} \right)^{1/4} D^{2/3} \sim 1.9 \frac{D^{2/3} U_g^{1/4}}{d^{1/2}} \tag{5}$$

independent of the electrode dimensions. For a constant bubble diameter, this predicts a very slow increase in mass transfer coefficient with current density, proportional to j^p with $p = 1/4$. Larger bubbles disperse more effectively, giving thicker gas plumes and a lower mass transfer coefficient.

For laminar natural convection, an exact analytical solution was recently derived [67] analogous to a solution known from thermal natural convection [68–70] but including the effect that a non-zero gas fraction has on the mixture viscosity, density, and hydrodynamic dispersion:

$$k_{lam} \approx \frac{0.68 D^{2/3} \left(\frac{g U_g}{\nu D_b^{1/3} z} \right)^{1/5}}{\left(1 + 1.2 \left(\frac{\nu U_g^4 z}{g D_b^3} \right)^{1/5} \right)^{1/3}} \tag{6}$$

This develops from a slowly increasing function $k_{lam} \propto U_g^{1/5}$ at very low gas flux to a very slowly decreasing $k_{lam} \propto U_g^{-1/15}$ as can be seen in Fig. 4.

For very low current densities, these corrections are small and we take the denominator in the expression of Eq. (6) to be one. Inserting Eq. (4) gives (see footnote)

$$k_{lam} = 0.83 D^{\frac{2}{3}} \left(\frac{g^{\frac{2}{3}} U_g}{\nu^{\frac{2}{3}} d_b h} \right)^{\frac{1}{5}} \approx 7.1 D^{\frac{2}{3}} \left(\frac{U_g}{d_b h} \right)^{\frac{1}{5}} \tag{7}$$

Under most conditions turbulent mass transfer coefficient will be larger than the laminar one.

In Fig. 4 we compare the relations for natural convection with the data for hydrogen bubbles in alkaline electrolytes. The inset shows how a_{ref} continues to decrease with increasing gas flux U_g, in contrast with the behaviour for oxygen bubbles in H_2SO_4 shown in Fig. 3.

Natural convection flow dominates the mass transfer, as evidenced by the good agreement between several of the literature results and the turbulent result of Eq. (5), both with horizontal and vertical electrodes.[3]

We note that most of the data in Fig. 4 shows no sign of significant micromixing. This is consistent with a low value of $a = 0.14$ that was previously observed for hydrogen bubbles in alkaline electrolytes under forced-flow conditions [33]. Only the data of Refs. [12,55] above roughly 1 A/cm^2 seem to tend to $a_{ref} \approx 1.2$ and 1.4, respectively, likely due to coalescence induced by the high surface coverage at these high current densities.

While for hydrogen-evolving cathodes in H_2SO_4, the mass transfer is found to be dominated by micromixing, for hydrogen evolution in alkaline electrolytes natural convection mass transfer usually prevails. Only around roughly 1 A/cm^2 some sources in Fig. 4 seem to show hints of micromixing becoming relevant. From Table 1 we see something similar for oxygen bubbles, with low powers of $p = \partial \ln k / \partial \ln j < 0.4$ only for very low current densities, a power around $p \approx 0.5$, typical for micromixing, at intermediate current densities, but also some values $p > 0.65$ for high current densities. Because both micromixing and natural convection seem necessary to explain most of the data for oxygen, we will now look at how to combine these effects.

4. Combining hydrodynamic- and micromixing (O_2)

4.1. Model

To describe the different powers in Table 1 for different current density ranges, especially prevalent for oxygen-evolving anodes, we require a model that can describe this transition from natural convection-dominated mass transfer at low current densities, to micromixing at higher current densities. The model of Ref. [33] describes the effect of micromixing in case the mass transfer is dominated by forced flow. In Appendix C we generalise this model to include also the limit in which micromixing dominates and find

$$k \approx k_f + \frac{k_\mu}{\sqrt{1 + \left(4 a \theta k_f / k_\mu\right)^2}} \tag{8}$$

[2] The final expression results after inserting the usually fine approximation $g/\nu \approx 10^7$ m^{-1}s^{-1} so that the prefactors 1.9 and 7.1 in Eqs. (5) and (7) respectively, have units m$^{-1/12}$s$^{-1/12}$, m$^{-2/15}$s$^{-2/15}$, and m$^{2/15}$s$^{2/15}$, respectively .

[3] The underpredicted literature results have very small electrode diameters of 1.12 cm [63], 3.3 mm [12], and 3.1 mm [55] so that edge-effects become important.

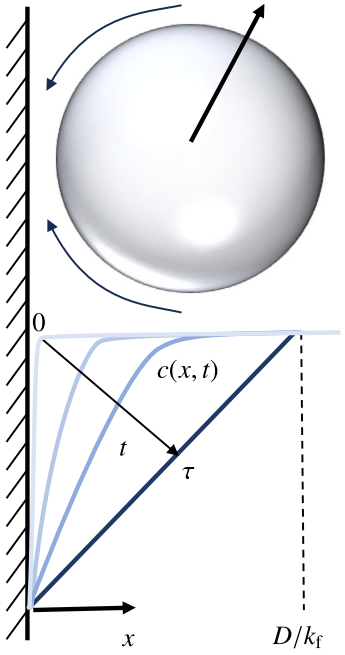

Fig. 5. An illustration of the surface renewal model of the micromixing mechanism of Ref. [8], refined in Refs. [11,32,33,71]. A coalescing, sliding, or departing bubble is assumed to mix the electrolyte. This gives a reactant concentration equal to the bulk concentration at $t = 0$. Next, a boundary layer starts to grow according to the transient diffusion equation. For a product, its concentration would decrease away from $x = 0$. After a time $t = \tau$, a steady boundary layer thickness D/k_f dictated by the flow mass transfer coefficient k_f is established.

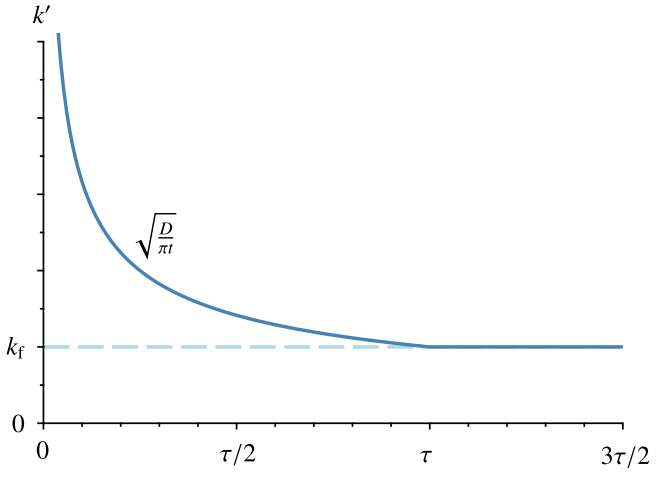

Fig. 6. The local mass transfer coefficient k' as a function of time after the departure of a bubble, modelled using the one-dimensional diffusion equation analytical solution. After a time τ this equals the background flow mass transfer coefficient k_f, which is then assumed to take over.

Note that this is a quite different result from the often-used simple averaging rule $k^q = k_f^q + k_\mu^q$, where Ref. [28] used $q = 1$ and Ref. [29] proposed $q = 2$. In space, the fractional electrode area $a\theta$ that is impacted by micromixing is used in the averaging. In time, the period in which micromixing dominates the background mixing is also consistently used in the averaging procedure. Therefore, we expect Eq. (8) to give more accurate results.

With respect to optimising mass transfer we note that since both k_μ and k_f increase with increasing current density, in general the mass transfer coefficient k will also increase with increasing current density.

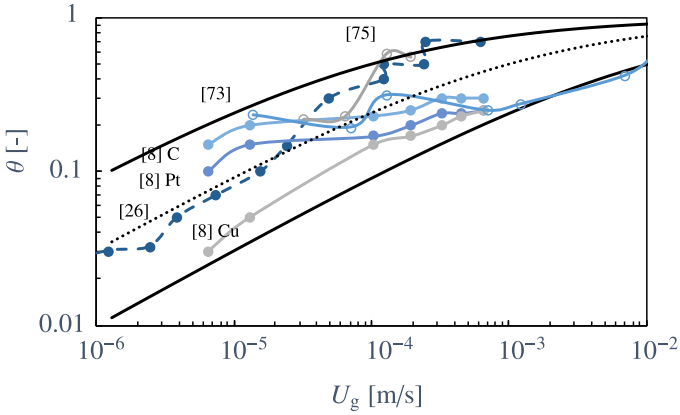

Fig. 7. The surface coverage θ of hydrogen bubbles in H_2SO_4 (solid circles) on vertical electrodes (solid lines) and horizontal electrodes (dashed lines). The open circles indicate alkaline electrolytes NaOH and KOH. The black lines indicate Eq. (10) with $r = 0.5$ and $j_c = 10^{-4}$ (top solid line), 10^{-3} (middle, dotted) and 10^{-2} A/m^2 (bottom, solid), respectively. The top and line of Ref. [8] used a carbon electrode and platinum electrode, respectively and would fit better with a still lower power $r \approx 0.15$ and $r = 0.2$, respectively [73].

Furthermore, since $k_\mu \propto \sqrt{\theta}$, Eq. (8) predicts that a higher surface coverage leads to increased mass transfer.[4]

Assuming $a\theta$ is at most of order one, Eq. (8) gives that macro-mixing dominates micromixing when $k_f \gg k_\mu$, or when.[5]

$$a^4\theta^2 U_g \lesssim 3 \cdot 10^{-6} \text{ m/s} \tag{9}$$

This requires either small current densities, so U_g and the surface coverage θ are small, or a small impact parameter a. For hydrogen bubbles in sulphuric acid, we found micromixing to dominate for all current densities, so a is not small, in agreement with the result of Fig. 3 for $a_{ref} = a\sqrt{(200\ \mu\text{m})\theta/d} \approx 1$. For hydrogen bubbles in alkaline electrolytes, we found no effect of micromixing in Fig. 4 up to high current densities corresponding to $U_g \approx 10^{-3}$ m/s. From Eq. (9), this shows that $a\sqrt{\theta} \lesssim 0.23$ in agreement with the value $a = 0.14$ found in Ref. [33] in a forced flow experiment. This very large difference in impact parameter between H_2SO_4 and KOH/NaOH is very surprising and shows something is fundamentally different between hydrogen evolution in these electrolytes. We will come back to what could explain this difference in Section 5. First, we will investigate the surface coverage θ required in Eq. (8) for considering the combined effect of flow and micromixing.

4.2. Bubble surface coverage θ

An often-used expression for the surface coverage was proposed in Ref. [72] obtained from correlating data from various sources. However, no distinction was made between whether gas evolved from an anode or a cathode, or the type of electrolyte. Therefore, here we have another look at the literature data to see if a more refined picture can be obtained.

Fig. 7 shows data for hydrogen bubbles, mostly for horizontal electrodes in H_2SO_4. However, the few references that include data

[4] This does not include the effect of surface coverage on k_f and a, which is likely usually positive. However, there may be exotic circumstances on hydrophobic electrodes, where a high surface coverage creates very large bubbles that impede flow and damp micromixing.

[5] Inserting Eqs. (1) and (5) gives $a^4\theta^2 U_g \ll 0.49\sqrt{\frac{\pi}{6}}\left(\frac{gD^2}{\nu}\right)^{\frac{1}{12}}$. Because of the very weak dependence on D and ν we may insert typical values $D^2/\nu \approx 10^{-12}$ m^2/s to obtain Eq. (9).

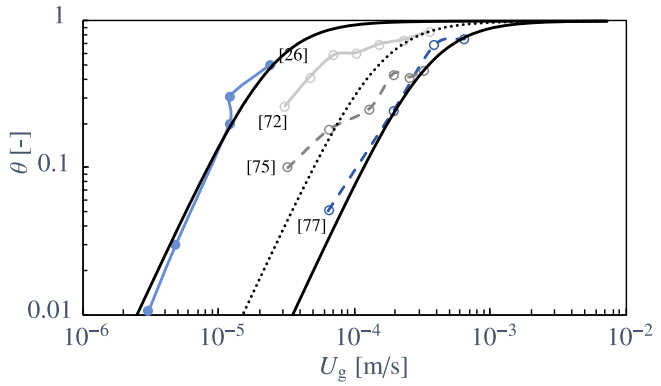

Fig. 8. The surface coverage θ of oxygen bubbles in KOH or NaOH (open circles) on vertical electrodes (dashed lines) and horizontal electrodes (solid lines). The dataset with closed circles was for H_2SO_4. The black lines indicates Eq. (10) with $r = 2$ and $U_\theta = 2.5 \cdot 10^{-5}$ m/s (top, solid line), $U_\theta = 1.5 \cdot 10^{-4}$ m/s (middle,dotted line), and $U_\theta = 3.5 \cdot 10^{-4}$ m/s (bottom, solid line). For Refs. [71,76] we only included the results at atmospheric pressure, no net liquid flow, and for decreasing current density [77].

for vertical electrodes or alkaline electrolytes show similar behaviour. Following Ref. [32] we use the following fitting function

$$\frac{\theta}{1-\theta} = \left(\frac{U_g}{U_\theta}\right)^r \tag{10}$$

where U_θ is a characteristic superficial gas velocity for which $\theta = 1/2$. A power $r = 0.5$ and U_θ between $10^{-4} - 10^{-2}$ m/s seems to fit most of the literature data reasonably well. The differences in U_θ likely are primarily related to the roughness and wetting properties of the surface, evidenced, for example, by the differences observed in Ref. [8] for different electrode materials. The expression $\theta \approx 0.023 \left(\frac{j}{\mathrm{A/m^2}}\right)^{0.3}$ proposed in Ref. [72] would, at low coverage, be described by Eq. (10) with $r = 0.3$ and $U_\theta = 3.7 \cdot 10^{-2}$ m/s. It correlates some of the literature data in Fig. 7 reasonably well but does not account for the maximum gas coverage of $\theta = 1$.

Fig. 8 shows the surface coverage data that can be found in the open literature for oxygen bubbles, mostly in alkaline electrolytes, but also one result in H_2SO_4. These results can also be fit with the same Eq. (10), but with strikingly different fitting parameters. While a value of $r = 0.15 - 0.5$ works well for the hydrogen coverage data in Fig. 7, a much higher value of $r \approx 2$ is required to fit the oxygen data. This difference was already noted in Ref. [57], where below 50 A/m^2 visual estimates showed several per cent of hydrogen bubbles but virtually no oxygen coverage. What causes this big difference is up for speculation. Oxidation processes occurring at the anode gives an oxidation layer which is known to reduce the contact angle and make metal surfaces more hydrophilic [74,75]. The resulting smaller attractive surface tension force on bubbles could lead to the observed low surface coverage at low current densities. More differences that may play a role in differences between anodes and cathodes will be discussed in Section 5.

4.3. Data-model comparison

Fig. 9 shows the mass transfer data available in the literature for oxygen evolution in the alkaline electrolytes NaOH and KOH. Most of the lower current densities show a value of a_{ref} that decreases with increasing current density, signalling a power $p = \partial \ln k / \partial \ln j$ smaller than 1/2, as we found for hydrogen bubbles in alkaline electrolytes in Fig. 4. Therefore, we attributed this to mass transfer due to natural convection. Eq. (5) gives $k_{\mathrm{turb}} \propto U_g^{1/4}$ so that $a_{\mathrm{ref}} \propto U_g^{-1/4}$ in good agreement with the data. At higher current densities, the trend reverses, and a_{ref} not only becomes constant, as we have seen for cathodes in H_2SO_4, but increases with increasing current density. This can be

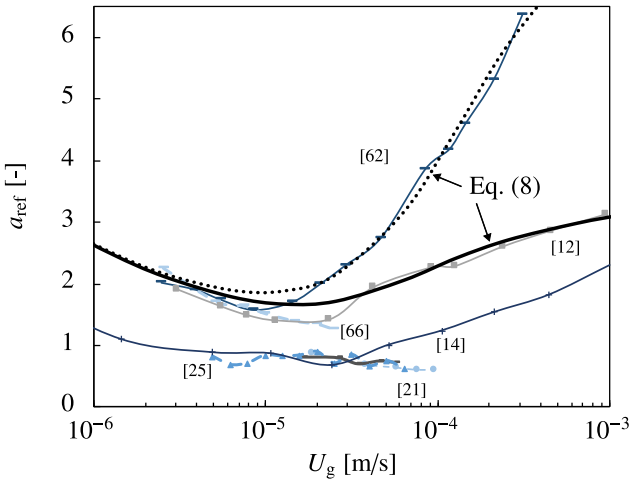

Fig. 9. The available literature data on mass transfer at oxygen-evolving electrodes in alkaline electrolytes. Solid lines represent horizontal electrodes and dashed lines are vertical ones. The dimensionless area impact parameter $a_{\mathrm{ref}} \equiv \frac{k}{\sqrt{\frac{6DU_g}{\pi d_{\mathrm{ref}}}}}$ depends non-monotonously on gas flux U_g. At low gas flux, natural convection dominates, while at higher gas flux, micromixing dominates. The solid line displays Eq. (8) with $a = 1.8$, using Eq. (5) for k_f, and Eq. (10) for the surface coverage θ with $r = 2$ and $U_\theta = 1.5 \cdot 10^{-4}$ m/s, corresponding to the dashed line in Eq. 8. This gives a good fit to the data of Ref. [12] for Nickel electrodes. The dotted line uses $a = 5$ and a slightly higher $U_\theta = 2.5 \cdot 10^{-4}$ m/s and fits well the data of Ref. [63] for Platinum electrodes.

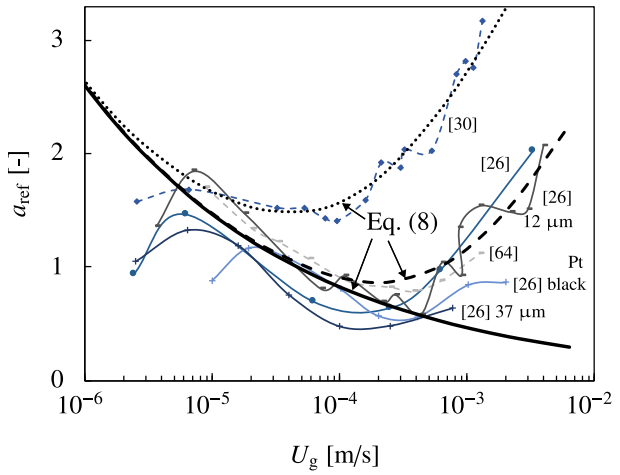

Fig. 10. The available literature data on mass transfer at oxygen-evolving electrodes in H_2SO_4 expressed in terms of the dimensionless area impact parameter $a_{\mathrm{ref}} \equiv \frac{k}{\sqrt{\frac{6DU_g}{\pi d_{\mathrm{ref}}}}}$. Solid lines represent horizontal electrodes and dashed lines are vertical ones. The black lines show Eq. (8) with Eq. (5) for k_f and Eq. (10) for the surface coverage θ with $r = 2$ and $U_\theta = 2.5 \cdot 10^{-5}$ m/s, corresponding to the top solid line in Eq. 7, best matching the data of Kind for H_2SO_4. The solid line represents purely natural convection and no micromixing ($a_{\mathrm{ref}} = 0$). The dashed line uses an ad-hoc fit $a_{\mathrm{ref}} = \ln\left(1 + U_g/U_c\right)$ with $U_c = 2 \cdot 10^{-3}$ m/s as a characteristic superficial gas velocity for which micromixing increases a_{ref} by a value $\ln 2 \approx 0.69$. The dotted line represents $a_{\mathrm{ref}} = 0.5 + \ln\left(1 + U_g/U_c\right)$ with $U_c = 5 \cdot 10^{-4}$. We note that we excluded the data of Ref. [63] which gives an unexplained anomalously high value of $a_{\mathrm{ref}} \approx 5$, approximately independent of U_g. For Ref. [57] the grain size of the sanding paper used for treating the platinum electrodes is indicated.

attributed to the bubble surface coverage θ increasing with increasing current density. In agreement with Eq. (1) an increase in surface coverage gives increased micromixing even if a remains constant. Fig. 9 shows a comparison with our model Eq. (5), where for the surface coverage we use the fit shown in Fig. 8. The agreement between our model and the experiments of Refs. [12,63] is excellent. Therefore, the bend in the mass transfer coefficient as a function of current density,

Table 2
Approximate range of values of a_{ref} required to fit the literature data, comprehensively summarised in graphs 3, 4, 9, and 10, excluding the anomalously high $a_{ref} \approx 4-5$ found for O_2 in H_2SO_4 in Ref. [63] and a few data points above roughly 1 A/cm^2 in Refs. [12] and [55] requiring $a_{ref} \approx 1$.

a_{ref}	KOH/NaOH	H_2SO_4
cathode/H_2	<0.5	1-2
anode/O_2	1–5	$0\text{-}0.5 + \ln\left(1+\frac{U_s}{U_c}\right)$

Table 3
The first two rows give the literature values for the dependence of the surface tension γ [mN/m] on electrolyte concentration c [mol/l] [78] and the surface charge q. The H_2SO_4 concentration is assumed to be such that the pH is below the isoelectric point. The next two rows give the gradient of the electrolyte concentration c and the surface tension in the x direction pointing away from the anode or cathode, respectively. The final two lines give the direction of both the resulting Marangoni force, proportional to $\frac{\partial\gamma}{\partial x} = \frac{\partial\gamma}{\partial c}\frac{\partial c}{\partial x}$ and the electrical force $-q\frac{\partial\phi}{\partial x}$, which happen to be in the same direction.

	KOH/NaOH	H_2SO_4
$\partial\gamma/\partial c$ [μN m^2/mol]	2	0.5
Q [C]	−−	+
cathode $\frac{\partial c}{\partial x}$, $\frac{\partial\phi}{\partial x}$	+	+
anode $\frac{\partial c}{\partial x}$, $\frac{\partial\phi}{\partial x}$	−	−
cathode $\frac{\partial\gamma}{\partial x}$, $-Q\frac{\partial\phi}{\partial x}$	−−	+
anode $\frac{\partial c}{\partial x}$, $\frac{\partial\phi}{\partial x}$	++	−

noticed already in Ref. [57] for example, can be explained well by an increase in surface coverage with increasing current density.

Fig. 10 shows the mass transfer data available in the literature for oxygen evolution in the acidic electrolyte H_2SO_4. Again, at low current densities[6] the parameter a_{ref} decreases with increasing current density, in agreement with what is expected from natural convection. As in the case of alkaline electrolytes, there is a strong increase in a_{ref} with increasing current densities. However, in this case, this behaviour cannot be fitted well with a constant a. Therefore, there is likely another reason why a_{ref} increases so strongly with increasing current density. Because the increase coincides with the region of very high surface coverage, as shown in Fig. 8, it seems likely that strong bubble interactions and coalescence cause an increase in micromixing. In Fig. 10, we provide a fit for a_{ref} that describes this increase well.

5. Discussion

5.1. Differences in micromixing

The proposed model Eq. (8) describes most of the trends very well with only one independent fitting parameter a_{ref}. The other fitting parameters of the model relate to the surface coverage or the hydrodynamics and can be obtained by other direct measurements. In Table 2 we summarise the values of a_{ref} that were required to fit the literature data. The strongest micromixing is found for oxygen bubbles in the alkaline electrolytes KOH and NaOH, followed by hydrogen bubbles in the acidic H_2SO_4. Very little to no micromixing is observed for hydrogen bubbles in KOH/NaOH, while oxygen bubbles in H_2SO_4 only sometimes show micromixing above a critical current density.

Possibly related, we found a strong difference between oxygen and hydrogen in terms of bubble surface coverage. The hydrogen coverage increases much more gradually with increasing current density than that of oxygen in both alkaline and acidic electrolytes.

These observations align with the observed size differences between bubbles. On a small horizontal platinum electrode in Ref. [63] it was found that hydrogen bubbles in KOH and oxygen bubbles in H_2SO_4 are the smallest and only the latter increase in size with increasing current density. See Fig. 2. Oxygen bubbles in KOH are the largest, followed by hydrogen bubbles in H_2SO_4. The observed increase in bubble size with increasing current density was associated primarily with the occurrence of coalescence [63]. Therefore, it seems plausible that also the strong micromixing observed for O_2 in KOH and H_2 in H_2SO_4 are due to coalescence events. The observed virtual absence of coalescence for hydrogen bubbles in alkaline electrolytes [63] then explains how hydrodynamics can dominate the mass transfer in this case.

A natural follow-up question remains: why do hydrogen bubbles coalesce more than oxygen bubbles in H_2SO_4 but it is the other way around in alkaline electrolytes?

5.2. Electric force

Over a century ago, Coehn and Neumann [79] argued that an electrostatic force is responsible. In surfactant-free electrolytes bubbles below a pH of 2–3, the case for all H_2SO_4 electrolytes used in this work, are moderately positively charged while at higher pH, the case for all experiments with KOH and NaOH used in this work, they are strongly negatively charged [80]. The electric field, directed from anode to cathode, therefore, exerts a force away from the anode and towards the cathode in sufficiently acidic electrolytes and the other way around in more neutral or alkaline solutions. This is illustrated in Fig. 12 and the final two lines of Table 3 summarise the sign of the electrical force. Because the charge magnitude is largest in alkaline electrolytes, which have a pH far from the isoelectric point of pH 2–3, the largest electrical force is expected there, indicated by the double pluses and minuses.

A force towards the electrode can *directly* influence the detachment radius of bubbles through its force balance. The attractive surface tension force scales linearly with the bubble radius, while the electric force scales with the bubble surface, so its radius squared. Therefore, a repulsive electric force can cause growing bubbles to be released from the electrode at a size smaller than buoyancy or other forces would. Also, *indirectly* the electric force may influence the bubble size. An attractive electrostatic force can cause bubbles to remain close to the electrode, coalesce, and form larger bubbles, while a repulsive force would lead bubbles away from the electrode, avoiding coalescence. Comparing the last two lines of Table 3 with Table 2, we see that an electrical force can explain the differences in micromixing that we found. The relatively large negative surface charge in alkaline electrolytes leads to a strong repulsive force on hydrogen bubbles and a strong attractive force on oxygen bubbles, potentially explaining why micromixing and bubble sizes in these cases are, respectively, smallest and largest. A relatively small negative surface charge leads to the opposite situation in H_2SO_4, potentially explaining why hydrogen bubbles show more micromixing than oxygen bubbles in this case. Except perhaps for high current densities where the high surface coverage of oxygen bubbles could cause increased micromixing.

Ref. [44] found that simulations with an attractive electrical force and a bubble surface charge density in agreement with other literature could explain well the oscillation frequency observed for hydrogen bubbles on a platinum micro-electrode in H_2SO_4. However, more direct evidence of the effect of electric forces on bubble detachment is presently lacking. Therefore, we will continue with alternative or additional explanations of a contributing factor that arguably is even more plausible.

5.3. Electrowetting

In 1933 Kabanow and Frumkin [81] expressed their doubts about an explanation of bubble size in terms of an electric force. Using experiments at extremely low current densities, they showed that differences in bubble sizes could be explained by differences in contact

[6] We note that the lowest current densities used in Ref. [57], but also that of Ref. [48], show a small dip in a_{ref}. A potential explanation is that at these low current densities, very few bubbles form and a significant fraction of the gas is transported out in dissolved form.

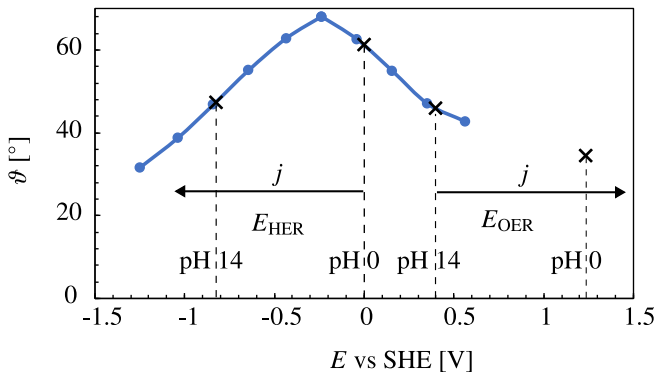

Fig. 11. Measurements of the contact angle ϑ [°] (through the liquid) of bubbles on platinum electrodes in 0.1 M Na_2SO_4, converted from Ref. [81] relative to a standard hydrogen electrode potential (SHE). Indicated are the reduction potentials E_{HER} (0 V) and E_{OER} (1.23 V) for the hydrogen evolution reaction and oxygen evolution reaction, respectively, at standard conditions for which pH = 0, but also at pH 14 by subtracting $14 \times \ln(10) RT/F \approx 0.83$ V. The black arrows indicate the direction in which the curve will be followed upon increasing the current density j.

angle through the phenomenon of electrocapillarity or electrowetting. Differences in potential on anode and cathode lead to differences in contact angle and, therefore, the adhesive force and departure size. Ref. [82] measured the contact angle as a function of voltage on various metals, and Fig. 11 shows the measurements of Ref. [81] for a platinum electrode. We indicated also the standard equilibrium potentials of the hydrogen and oxygen evolution reactions, where we note that upon applying a finite current cathodic currents will become negative and anodic currents will become more positive due to activation overpotentials. Therefore, except perhaps for hydrogen in strong acidic electrolytes at very low overpotentials, the bubble contact angle on this electrode will decrease with increasing current density. In the absence of coalescence, such smaller contact angles would lead to smaller bubble departure diameters. A similar decrease in hydrogen bubble contact angle from about 45° to 35° with increasingly negative potentials was found in Ref. [43] for platinum micro-electrodes that were smaller than the bubble size in H_2SO_4.

There are several indications from the literature that electrowetting may play a role.

Ref. [83] finds a small decrease in both oxygen and hydrogen bubble size with increasing current density below 100 A/m^2 or $U_g \approx 10^{-5}$ m/s. Ref. [84] also finds the bubble size decreases with increasing current density. Additionally, hydrogen bubbles decrease in size with increasing pH while the size of oxygen bubbles increases with increasing pH, in perfect agreement with the predictions from electro-wetting and an electrocapillary curve like that shown in Fig. 11.

Increasing the pH shifts the reduction potentials to the left. This leads to an increase in contact angle for oxygen bubbles but usually to a decrease for hydrogen bubbles, in agreement with the trend in bubble size at low current densities of Fig. 2. We note that there may be very large differences between the ‘equilibrium contact angles’ depicted in such electrocapillary curves and the advancing contact angles that occur for growing bubbles due to contact line pinning. Ref. [85], for example, found the contact angle of a single bubble to decrease from about 70° to 20°.

Electrocapillary curves like that shown in Fig. 11 depend on the solid surface and usually, to a lesser degree, also the liquid properties. Therefore, a different curve is expected for Nickel electrodes in KOH. However, the point of zero charge, the location of the maximum in Fig. 11, is similar for Nickel and platinum [86].

In general, relatively large potential changes are required for modest changes in contact angle. Therefore, while electrocapillarity may play a role in bubble size, other, more important effects may exist. Due to higher surface coverage or the attractive electric force discussed in the previous sub-section, coalescence can lead to the often observed increase in bubble size with increasing current density. Therefore, these two opposing effects may resolve the various conflicting statements in the literature on whether the size of bubbles increases or decreases with increasing current density.

However, there are also various other observations related to bubble size and micromixing that the hypothesis of a dominant electric force has difficulty explaining.

5.4. Other bubble phenomena

While wetting phenomena like electrowetting may be able to explain the size differences between bubbles at very low current densities, various phenomena require the existence of an additional force. For example, the phenomenon of “radial specific coalescence” found for oxygen bubbles in alkaline media [87] in which smaller bubbles move over several bubble diameters radially towards a larger bubble that collects them. Subsequently, these oxygen bubbles were found to remain very close to the electrode while rising as if attracted to the electrode. During their rise, they are observed to grow further by “scavenging” attached bubbles [88]. On the other hand, hydrogen bubbles in alkaline electrolytes seem to ‘glide’ over a layer of attached bubbles [76] with which there is very little interaction, as if there is a repulsive force in this case. In acidic electrolytes it are the hydrogen bubbles that show scavenging [88], sometimes also showing sideways oscillations as if influenced by some periodic force [63].

Coalescing bubbles can jump away from the surface because of the momentum imparted by their changing centre away from the electrode. Under alkaline conditions, coalesced oxygen bubbles were found to jump away from the surface almost exclusively when both are larger than 50 μm in diameter [42]. Furthermore, coalescence-induced jump-off was found to occur with a greater probability for larger and more similarly sized bubbles [89]. Simulations [38] showed coalescence-induced departure only below a contact angle of 35°. Surprisingly, sometimes, the coalesced bubble has been observed to return to the electrode shortly after [90]. This “Bubble jump-off and return” seems to require some force, be it hydrodynamic or otherwise, to be explained. Interestingly, as with the scavenging, oscillations, and radial coalescence, the attractive force also underlying this phenomenon has only been observed for hydrogen bubbles in H_2SO_4 [90,91], or oxygen bubbles in KOH [87].

Finally, above a critical current density hydrogen bubbles in H_2SO_4 were found to detach and oscillate float on top of a ‘bubble carpet’ [44]. While this study provides as a conclusive explanation an electrostatic attractive force, the effect of electrocapillarity was omitted [92] warranting further study and potentially a different origin of the observed attractive force.

5.5. Marangoni forces

Electric forces or oscillations after coalescence [87] were posed as explanations for bubble return after jump-off. Also, inertial lift forces and further coalescence with smaller bubbles can sometimes explain bubble movement towards the wall [39,93]. Upon its first discovery in Ref. [90], bubble return to the electrode was actually speculated to be due to surface tension-gradient driven flows. Gradients in temperature, electrolyte concentration, or potential can cause differences in surface tension over the bubble surface, setting its interface and the surrounding fluid into motion. These flows are called solutal, thermal, or electrocapillary Marangoni flows, depending on their origin.

We do not consider electrocapillary Marangoni flows here, as it predicts a force that is in the opposite direction as the electrostatic force. For a spherical bubble with constant surface charge in an infinite medium, we show in Appendix D that it merely acts to cancel half of the electrostatic force. While this could be different for a real bubble near

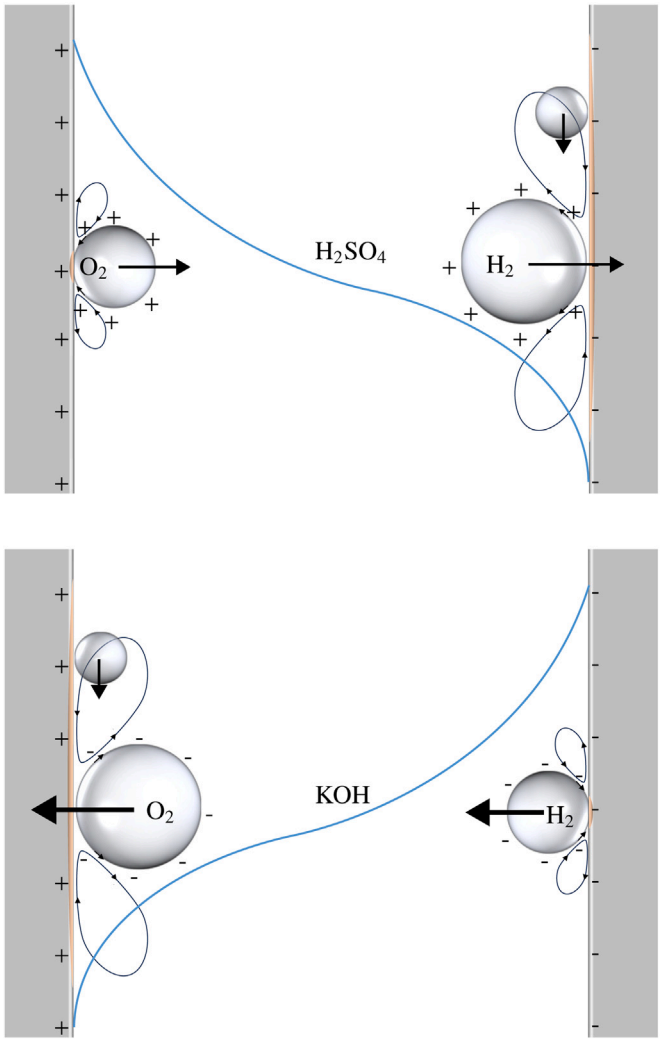

Fig. 12. A schematic of the bubble forces (arrows), concentration profile c (blue line), and solutal Marangoni flows (lobes near bubbles) near the anode (left) and cathode (right) in an alkaline (top) and acidic (bottom) electrolyte assuming a positive surface tension increment $\partial\gamma/\partial c$. Both electric forces and Marangoni forces may force oxygen bubbles in alkaline and hydrogen bubbles in acidic electrolytes towards the electrode, but only the latter can attract surrounding bubbles. The orange region roughly indicates the area $a\theta A$ impacted by micromixing, similar to Fig. 1. (For interpretation of the references to colour in this figure legend, the reader is referred to the web version of this article.)

an electrode, we do not expect this force to be helpful in explaining the above phenomena.

Most often solutal and thermal Marangoni forces are assumed to be relevant, where concentration gradients due to dissolved gases and electrolyte have been considered. We note that previous claims that dissolved hydrogen or oxygen gas can lead to Marangoni convection [94] have been contested using the argument that on the surface of a bubble, the gas-vapour thermodynamic equilibrium precludes concentration gradients over the surface [95]. While temperature gradient-driven Marangoni flows can play a role [96], especially on micro-electrodes with very high voltages [45,95], under water-electrolysis conditions electrolyte concentration gradients are likely to be more important. In Appendix D we estimate that, for bubbles in H_2SO_4, solutal Marangoni forces dominate below about 0.8 V of electrode overpotential. This is in agreement with the estimates of Ref. [45] and is usually the case in experiments with macroscopic electrodes. In KOH and NaOH, we estimate in Appendix D that the solutal Marangoni force dominates up to 5 V of overpotential so that thermal Marangoni forces can almost always be safely neglected.

In Fig. 1, we illustrate how electrolyte concentration gradients lead to Marangoni flows and forces on bubbles near an electrode. in H_2SO_4, due to the consumption of protons, the electrolyte concentration is lower at the cathode surface, giving rise to a surface tension gradient over the surface of a bubble that drives a flow away from the surface, pushing hydrogen bubbles towards the electrode. This additional force could lead to the accumulation of small bubbles, consequent coalescence, and periodic detachment of relatively large bubbles. Therefore, it can explain the larger size of hydrogen bubbles compared to oxygen bubbles in H_2SO_4.

This seems to have been little considered so far, and overlooked in Ref. [97], but under alkaline conditions, using KOH and NaOH as electrolytes, the electrolyte concentration increases instead of decreases towards the electrode surface because (OH^-) ions are produced rather than (H^+) being consumed. This means that the direction of Marangoni flows and the associated force are reversed, pushing hydrogen bubbles away from the surface. Because bubbles do not stick around and coalesce, the resulting bubbles are much smaller. The various possibilities are summarised in Table 3.

Because of this difference in the direction of electrolyte concentration in alkaline versus acidic electrolytes, solutal Marangoni forces predict a qualitatively similar effect on oxygen bubbles in alkaline electrolytes and hydrogen bubbles in acidic electrolytes. Since concentration gradients increase with increasing current density, solutal Marangoni forces play an increasing role at increasing current density. Since the variation in surface tension with concentration is about four times larger [78] in KOH and NaOH compared to in H_2SO_4 larger effects are expected of solutal Marangoni forces in these alkaline electrolytes. This is exactly what we found for the degree of micromixing on various electrodes and electrolytes. It can also explain why oxygen bubbles in alkaline electrolytes are largest at elevated current densities and hydrogen bubbles are smallest as illustrated in Fig. 2.

As illustrated in Fig. 12 and Table 3, electric forces could, in principle, predict the same trends, but there are several reasons why solutal Marangoni forces seem to have a larger explanatory power. Unlike Marangoni forces, electric forces have only been inferred very indirectly and may actually be partly or largely cancelled by electrocapillary Marangoni flows. For example, Ref. [47] shows, supported with high resolution and frequency images, the return of a bubble to be due to Marangoni forces. Electrical effects could be excluded because the reversal also occurred when the electric field was absent between release and return. Electric forces would predict a change in the direction of the force around the isoelectric pH of 2–3, while solutal Marangoni forces change direction around a pH of 7. While not conclusive, the data of Ref. [97] seems to show more of a trend change in the latter pH range. Finally, unlike the electrostatic force, the radial influence of Marangoni flows can also explain why phenomena like bubble jump-off and return, floating on bubble carpets above a certain critical current density, and radial coalescence. These phenomena have been observed for hydrogen bubbles in acidic electrolytes and not for oxygen bubbles. In alkaline electrolytes, various of these effects have been found only for oxygen bubbles, exactly as predicted for an attractive force due to Marangoni convection.

5.6. Coalescence

What remains to be explained is the enhanced micromixing that is observed for oxygen bubbles in H_2SO_4 shown in Fig. 10 and the strong increase in bubble diameter with increasing current density shown in Fig. 2. The reason here may very well be coalescence, induced not by an additional force but by a high surface coverage. In case the whole electrode is filled with bubbles, coalescence can no longer be avoided, even in the presence of a mild repulsive force. From Fig. 8, the increase in bubble size takes place around the same $U_g \gtrsim 2 \cdot$

10^{-5} m/s for which the surface coverage increases to 0.5 [57]. Such high values of surface coverage occur at much higher values $U_g \gtrsim 10^{-4}$ m/s in all other cases.[7] The reason for the strong increase in surface coverage with increasing current densities on anodes shown in Fig. 8, especially in acidic electrolytes, compared to the much more gradual increase observed for hydrogen bubbles in Fig. 7 is an open question but likely relates to wetting properties of the surface. Oxidation may increase wetting, but electrowetting may play an additional role.[8] An outstanding challenge for future research will be to provide more insight into the observed values of the parameter a_{ref}. When two bubbles of diameter d coalesce, because at least the area below the two bubbles will be effectively mixed, the corresponding a will likely be at least 2 and potentially much larger due to the large flows arising due to coalescence [17,102,103]. Therefore, values of $a_{ref} > 1$ may be explained by coalescence events. Sliding of bubbles along the electrode can in theory also strongly increase a beyond 1 as the area of the sliding path can be many times the area under a bubble [104].

6. Conclusions

Micromixing at gas-evolving electrodes can be conveniently described in terms of the dimensionless parameter a, which denotes the area around a bubble effectively refreshed upon its release relative to the area under a bubble according to Eq. (1). We investigated a related quantity a_{ref}, defined in Eq. (3), which assumes a reference bubble size and surface coverage. By comprehensively analysing the relevant mass transfer data from the literature, we find that this parameter, representative of the degree of micromixing, is always quite small for hydrogen bubbles in alkaline electrolytes and for oxygen bubbles in H_2SO_4 at low current densities. Therefore, this allows us to describe the mass transfer in these cases using the analytical expressions for laminar and turbulent natural convection summarised in Section 3. Fig. 4 shows how several relatively short vertical electrode literature results are described well using a laminar mass transfer relation recently obtained [67] and several horizontal results and several horizontal or very long vertical electrode results are described well using the turbulent relation of Eq. (5) that we derived here using the Chilton–Colburn analogy.

As shown in Section 5, the value of a_{ref} required to fit the data for hydrogen bubbles in H_2SO_4 and especially oxygen bubbles in KOH/NaOH were much larger. These trends fully agree with the observed differences in bubble size at elevated current densities, making it likely that both bubble size and micromixing are dominated by coalescence at elevated current densities. While electrowetting seems to be able to explain the size differences at low current densities, an additional force seems to be required to explain these results at higher current densities. Both the electrostatic force and a force due to electrolyte concentration gradient-driven Marangoni flows can explain the differences between oxygen and hydrogen in acidic and alkaline electrolytes as can be seen by comparing Tables 2 and 3. While both forces may contribute, solutal Marangoni flows seem more suited to explain also a variety of other bubble behaviour observed. Something that requires further explanation is the rapid growth of oxygen bubbles in H_2SO_4 with increasing gas flux, shown in Fig. 2, despite a presumed repulsive force. By analysing the literature data, we find in Fig. 8 that the surface coverage of oxygen bubbles, especially in H_2SO_4, grows rapidly to high values with increasing gas flux. The coalescence induced by this high surface coverage likely explains the larger bubble size and increased micromixing observed in Fig. 10 beyond a certain gas flux.

Finally, we proposed a relatively simple mass transfer coefficient relation Eq. (8) that allows combining micromixing and mass transfer from natural convection in a physically consistent manner. Using only a_{ref} as an independent fitting parameter, this relation describes most of the literature data quite well. Therewith, the long-standing challenge of uniting mass transfer due to micromixing with that due to natural convection flows at gas-evolving electrodes was successfully resolved.

CRediT authorship contribution statement

J.W. Haverkort: Writing – review & editing, Writing – original draft, Visualization, Validation, Methodology, Investigation, Formal analysis, Data curation, Conceptualization.

Declaration of competing interest

The authors declare that they have no known competing financial interests or personal relationships that could have appeared to influence the work reported in this paper.

Acknowledgement

This publication is part of the project “Hydrogen bubbles quantified" (Vidi grant with project number 19665) which is (partly) financed by the Dutch Research Council (NWO). I gratefully acknowledge preliminary discussions on mass transfer with N. Valle.

Appendix A. Micromixing

We re-derive here for convenience the micromixing expression presented as new in [71], which however only differs by a factor $\sqrt{\frac{1}{18}\frac{\theta}{1-\theta}}$ from that in Ref. [8]. It was extended to include forced flow in Refs. [32,33] and various types of bubble behaviour in Ref. [104].

We assume that after a bubble departs, the fluid around a bubble is completely mixed so that the concentration is constant. A concentration boundary layer arises, which grows in time. The analytical solution of the transient one-dimensional diffusion equation gives a (Cotrell) mass transfer coefficient $\sqrt{D/\pi t}$ that decreases inversely proportional to the square root of time. The *time-averaged* and local mass transfer coefficient over a bubble cycle time t_d reads

$$k'_\mu \equiv \frac{\int_0^{t_d} \sqrt{D/\pi t}\, dt}{t_d} = 2\sqrt{\frac{D}{\pi t_d}} = \sqrt{\frac{4DU_gA}{\pi V_b}}, \tag{A.1}$$

where we wrote the volumetric gas flux as $U_g = V_b/At_d$, in terms of the combined adhering bubble volume V_b and electrode area A. The prime here indicates that this is a time-averaged local quantity near the bubble, not yet averaged over space.

We will write the area that is effectively mixed by departing bubbles as $a\theta A$, where θA is the combined projected electrode area below or ‘in the shadow’ of the bubbles. The dimensionless parameter a thus gives the electrode area affected by the bubble relative to the bubble surface coverage. For spherical bubbles of diameter d we have $\theta A/V_b = \frac{\pi d^2/4}{\pi d^3/6} =$

[7] Such surface-coverage induced coalescence may also be the cause of the strong increase in micromixing observed for hydrogen bubbles in H_2SO_4 for $U_g \gtrsim 10^{-2}$ m/s, see Fig. 3. The data in Fig. 7 makes it plausible that only at such extremely large gas fluxes the surface coverage reaches similarly high values of around 0.5.

[8] The Young–Lippman equation predicts that the liquid–solid interfacial tension decreases quadratically with the voltage deviation from the potential of zero charge [98]. However, sometimes asymmetric curves are obtained due to the onset of contact angle saturation with often higher saturation contact angles for anodic potentials for which various explanations exist [99–101]. Also, in the data of Fig. 11, the data point for most positive potentials may hint at saturation. Admittedly speculative, such a high contact angle could contribute to a larger bubble size with increasing current density. The stronger attractive surface tension force at elevated current densities leads to larger and more bubbles, increasing the coverage. At cathodes, the contact angle decreases with increasing current density, leading to smaller bubbles repelled from the electrode in alkaline electrolytes and sticking to the electrode, coalescing and being scavenged by or radially attracted to larger bubbles in acidic electrolytes.

$3/2d$. Averaging over the electrode area multiplies Eq. (A.1) with $a\theta$ to give the overall mass transfer coefficient as

$$k_\mu = a\theta k'_\mu = a\sqrt{\frac{4DU_g\theta}{\pi}\frac{\theta A}{V_b}} = a\sqrt{\frac{6DU_g\theta}{\pi d}}, \tag{A.2}$$

where in the final expression, we assumed equal-sized spherical bubbles of diameter d. When micromixing is dominated by coalescence, d may still be taken to represent the departure diameter. The surface coverage θ then only concerns the bubble area of the final departing bubbles. Since the largest bubbles have the largest weight in this area measure, this difference should not lead to large errors.

Appendix B. Hydrodynamic mass transfer

Lévêque approximation. The Lévêque approximation makes use of the fact that usually in liquids the mass diffusion coefficient $D = O\left(10^{-9}\right)$ m^2/s is much smaller than the kinematic viscosity $\nu = O(10^{-6})$ m^2/s. Therefore, the mass transfer boundary layer is much thinner than the hydrodynamic boundary layer, and the velocity in the z-direction parallel to the electrode $w(z) \approx w'x$ can be linearised in the x-coordinate normal to the electrode. In this case, it can be shown that the mass transfer coefficient can be given by [67].

$$k_f = \left(\frac{D^2}{9\int w'^{-1}dz}\right)^{1/3}. \tag{B.1}$$

Analogy with thermal natural convection. An analogy with thermal natural convection will allow us to equate the relative density (ρ) gradient due to differences in temperature T to the gradient in the gas fraction ϵ according to

$$\frac{\nabla\rho}{\rho_l} = -\beta\nabla T = \frac{\beta\mathbf{q}_h}{\lambda} \leftrightarrow -\nabla\varepsilon = \frac{\mathbf{U}_g}{D_b}. \tag{B.2}$$

Here, the first equality assumes the commonly used Boussinesq approximation, with β [m^3/K] the thermal expansion coefficient. The second equality expresses Fourier's law, with $\mathbf{q}_h$ [W/m^2] the heat flux. The final equality assumes that the volumetric gas flux at the wall $\mathbf{U}_g$, oriented away from the wall, is transported out by diffusion with a bubble dispersion coefficient D_b.

Analogy between transport of heat, mass, and bubbles. The Chilton–Colburn analogy provides a relation between heat transfer coefficients k_{heat} and flow mass transfer coefficient k_f

$$\frac{k_{heat}/\rho c_p}{\alpha^{2/3}} \approx \frac{k_f}{D^{2/3}} \approx \frac{k_{bubble}}{D_b^{2/3}}, \tag{B.3}$$

where we define the *bubble transfer coefficient* as $k_{bubble} = U_g/\Delta\varepsilon$ and $\alpha = \lambda/\rho c_p$ [m^2/s] is the thermal diffusivity, with λ [W/m/K] the thermal conductivity and ρc_p [J/m^3/K] the volumetric heat capacity at constant pressure. The analogy uses that diffusion of heat and mass is similar as long as they share the same velocity field. Note that the Lévêque result of Eq. (B.1), when applied to transport of heat, mass, or bubbles, automatically satisfies Eq. (B.3). Also, in turbulent flow, the equivalence between diffusion of heat and mass makes Eq. (B.3) usually a good approximation.

Turbulent natural convection. For turbulent flow, we can use Eqs. (B.2) and (B.3) to translate results from heat transfer to mass transfer. For upwards-facing heated horizontal surfaces, Ref. [105] gives an overview of the literature results and finds a heat transfer coefficient[9]

$$\frac{k_{heat}}{\alpha^{2/3}\rho c_p} = 0.175\left(\frac{g\beta\Delta T}{\nu}\right)^{1/3}. \tag{B.5}$$

[9] Eq. (B.5) agrees within roughly 20% with at least four independent measurements, over a wide range of Rayleigh numbers $3\cdot10^6 \le \frac{g\beta\Delta Th^3}{\nu\alpha} \le 10^{10}$ and was obtained for a constant temperature difference ΔT. The result for a constant heat flux q can be approximately obtained by replacing $\Delta T = q/k_{heat}$ and solving for k_{heat} to give

$$\frac{k_{heat}}{\rho c_p} = 0.27\left(\frac{g\beta q/\lambda}{\nu}\alpha^3\right)^{1/4} \tag{B.4}$$

In the range of modified Rayleigh numbers $3\cdot10^7 \le \frac{g\beta qh^4/\lambda}{\nu\alpha} \le 4\cdot10^{11}$ it has a maximum relative error of around 30% with the piecewise correlation provided in Ref. [106] for a constant heat flux. Refs. [107] for water and [108] for air found no difference between a horizontal and vertical orientation in the turbulent regime, except for the Rayleigh number at which the laminar-turbulence transition occurs. For water up to Rayleigh numbers of 10^{16}, Ref. [108] finds a power 0.24 and prefactor 0.302, very close to the coefficients in Eq. (B.4).

We use Eq. (B.3) to replace the left-hand side with $k_{bubble}/D_b^{2/3}$ and Eq. (B.2) to replace $\beta\Delta T$ with U_g/k_{bubble} so that

$$k_{bubble} = 0.27\left(\frac{gU_g}{\nu}D_b^2\right)^{1/4}, \tag{B.6}$$

where we used $0.175^{3/4} \approx 0.27$. Next, we invoke the Chilton–Colburn analogy $\frac{k_f}{D^{2/3}} \approx \frac{k_{bubble}}{D_b^{2/3}}$ to obtain

$$k_f = 0.27\left(\frac{gU_g}{\nu D_b^{2/3}}\right)^{1/4} D^{2/3}. \tag{B.7}$$

Appendix C. Combining flow and micromixing

Here, we re-derive and extend the model introduced in Refs. [32, 33]. We assume that after a bubble with diameter d has departed, its environment is effectively mixed and diffusion transiently restores the steady-state concentration gradient due to flow, as illustrated in Fig. 5. After a time τ, the Cotrell mass transfer coefficient $\sqrt{D/\pi t}$ has decreased to the level of the background flow mass transfer coefficient k_f so

$$k_f = \sqrt{\frac{D}{\pi\tau}} = \frac{k'_\mu}{2\sqrt{\bar\tau}}, \tag{C.1}$$

where $\bar\tau = \tau/t_d$ is the fraction of the bubble departure time for which micromixing exceeds the background mass transfer. After this phase, we assume that the local mass transfer coefficient is given by k_f and micromixing plays no role. We assume no waiting time or mixing time so that immediately after a bubble departs, the cycle starts anew with a constant concentration profile.

Assuming $\tau < t_d$, the local (indicated with a prime) mass transfer coefficient averaged over the bubble departure time t_d reads

$$k' = k_f(1-\bar\tau) + \bar\tau\frac{\int_0^\tau\sqrt{\frac{D}{\pi t}}dt}{\tau} = k_f(1+\bar\tau). \tag{C.2}$$

For $t < \tau$ the Cotrell mass transfer coefficient determines the local mass transfer coefficient and when $t > \tau$, the flow mass transfer coefficient takes over. In the second expression of Eq. (C.2), the factor two that arises from the integration is cancelled by the term $-k_f\bar\tau$ after invoking Eq. (C.1). Note that in this regime, micromixing doubles the background flow mass transfer coefficient at most.

In case $\tau > t_d$ and micromixing continues to dominate throughout the entire bubble cycle. In this case, we have $k' = k'_\mu$.

Next, we have to average over space. Here, we assume that micromixing plays a role over a fraction $a\theta$ of the electrode. For the rest of the electrode, we assume the flow mass transfer coefficient k_f prevails. The average mass transfer coefficient $k = (1-a\theta)k_f + a\theta k'$ gives

$$k = k_f + a\theta\times\begin{cases} k_f\bar\tau & \bar\tau < 1, \\ k'_\mu - k_f & \bar\tau \ge 1. \end{cases} \tag{C.3}$$

Because it is often more convenient to work with a continuous function, we provide the following approximation to Eq. (C.3)

$$k \approx k_\mathrm{f} + \frac{a\theta k'_\mu}{\left(1+\left(\frac{4}{\bar\tau}\right)^{\frac{s}{2}}\right)^{\frac{1}{s}}} \approx k_\mathrm{f} + \frac{a\theta k'_\mu}{\sqrt{1+16k_\mathrm{f}^2/k'^2_\mu}}, \tag{C.4}$$

where in the second expression we inserted $\bar\tau = k'^2_\mu/4k^2_\mathrm{f}$ and chose $s = 2$. The maximum relative difference with Eq. (C.3) of 12% seems acceptable given the heuristic nature of the model. Choosing $s = 2.5$ the difference would be 7%. The limiting result $k \approx k_\mathrm{f} + a\theta k'^2_\mu/4k_\mathrm{f}$ in case of dominant flow mass transfer $k_\mathrm{f} \gg k_\mu$ was obtained in Ref. [33] and successfully used to describe forced flow experiments. The usefulness of the result of Eq. (C.4) derived here is that it extends this result to include also the case $k_\mu \gg k_\mathrm{f}$ where micromixing dominates and $k \approx k_\mathrm{f} + a\theta k'_\mu$.

Appendix D. Marangoni forces

Thermal versus solutal marangoni forces. The Marangoni force on a bubble will be proportional to the changes in surface tension over its surface, for example, due to temperature differences ΔT or concentration differences Δc, giving for the ratio of the solutal and thermal Marangoni forces

$$\frac{F_{\mathrm{M},c}}{F_{\mathrm{M},T}} \approx \frac{\frac{\partial\gamma}{\partial c}\Delta c}{\frac{\partial\gamma}{\partial T}\Delta T}. \tag{D.1}$$

Both concentration and heat are generated at the electrode surface, proportionally to the current density, and are transported in a similar way, albeit with a different diffusivity. We write for the molar flux of hydroxide ions or protons $k\Delta c = f_D j/F$, where f_D denotes the fraction of the ion flux carried by diffusion, with $1 - f_D$ giving the fraction carried by migration. For the heat flux, we write $k_\mathrm{heat}\Delta T = j\eta$, where η will be close to the electrode overpotential. Inserting into Eq. (D.1) and invoking the Chilton–Colburn analogy of Eq. (B.3) gives

$$\frac{F_{\mathrm{M},c}}{F_{\mathrm{M},T}} \approx f_D \frac{\frac{\partial\gamma}{\partial c}}{\frac{\partial\gamma}{\partial T}} \frac{\rho c_p}{F\eta}\left(\frac{\alpha}{D}\right)^{2/3}. \tag{D.2}$$

To provide an estimate for dilute aqueous electrolytes, we use the properties of water at room temperature: a thermal diffusivity $\alpha \approx 1.4\cdot10^{-7}$ m^2/, volumetric heat capacity $\rho c_p \approx 4.2\cdot10^6$ J/m^3/K, and surface tension temperature dependence $\partial\gamma/\partial T \approx 1.6\cdot10^{-4}$ N/m. With the proton diffusion coefficient $D \approx 9.3\cdot10^{-9}$ m/s and $\partial\gamma/\partial c \approx 0.5$ μN m^2/mol measured for H_2SO_4. This gives *for sulphuric acid*

$$\frac{F_{\mathrm{M},c}}{F_{\mathrm{M},T}} \approx \frac{0.5\ \mathrm{V}}{\eta}. \tag{D.3}$$

In steady-state and in the absence of flow $f_D = \frac{1}{1+|z_\mathrm{m}/z_\mathrm{n}|}$ with z_m and z_n the charge numbers of the mobile and non-mobile ions [109], $z_\mathrm{m} = 1$ and $z_\mathrm{n} = -2$ for the H^+ and SO_4^{2-} in H_2SO_4, so that we used $f_D = 2/3$ in Eq. (D.3). While at the electrode surface, the conditions of steady-state and no flow may hold to a reasonable degree, this is clearly not true near the surface of the bubble. Advection may increase the contribution of migration so that Eq. (D.3) may be an upper estimate of $F_{\mathrm{M},c}/F_{\mathrm{M},T}$. Usually, in water electrolysis, the cathodic and anodic overpotentials are well below 0.5 V, so solutal Marangoni forces may dominate. Reference. [45] estimated thermal Marangoni effects to dominate over solutal effects at cathodic potentials below about −0.6 V for hydrogen bubbles in 1M H_2SO_4, in good agreement with our prediction. However, the assumptions used in both estimates are highly uncertain and require further scrutiny.

In the alkaline electrolytes KOH and NaOH the coefficient $\partial\gamma/\partial c \approx 2$ μN m^2/mol is significantly higher than in H_2SO_4. Also the OH^- diffusivity $D \approx 5.3\cdot10^{-9}$ m^2/s is lower than the proton diffusivity so that *in potassium or sodium hydroxide*

$$\frac{F_{\mathrm{M},c}}{F_{\mathrm{M},T}} \approx \frac{2.5\ \mathrm{V}}{\eta}. \tag{D.4}$$

For KOH and NaOH we have $z_\mathrm{m} = -1$ and $z_\mathrm{n} = 1$ so that we used $f_D = \frac{1}{1+|z_\mathrm{m}/z_\mathrm{n}|} = 1/2$ in Eq. (D.4). Therefore, according to this estimate, at normal water electrolysis overpotentials η, in the hundreds of mV range, thermal Marangoni forces can generally safely be neglected. But again, the assumptions underlying these estimates will require further scrutiny.

Marangoni versus electrostatic forces. For a spherical bubble moving in the Stokes flow regime in an infinite medium, an exact expression for the Marangoni force can be derived in case the surface tension varies linearly in a coordinate x along the flow direction [110,111]

$$F_\mathrm{M} = \frac{\pi d^2}{2}\frac{d\gamma}{dx}. \tag{D.5}$$

In the case of electrocapillary Marangoni flow we have $\frac{d\gamma}{dx} = \frac{d\gamma}{d\phi}\frac{d\phi}{dx}$ where the (Gibbs-)Lippmann equation [112] gives $\frac{d\gamma}{d\phi} = q$ [C/m^2], the surface charge density. Since the electrostatic force F_E is given by the product of the bubble charge $q\pi d^2/4$ and the electric field $-d\phi/dx$ we find relative for the relative electrocapillary Marangoni force

$$\frac{F_{\mathrm{M},\phi}}{F_\mathrm{E}} = -\frac{1}{2}. \tag{D.6}$$

So the electrocapillary Marangoni force on a small spherical bubble in an infinite medium is half the magnitude of the electric force and acts in the opposite direction so cancels half of the electric force.

References

[1] Sides Paul J. Phenomena and effects of electrolytic gas evolution. In: Modern aspects of electrochemistry. Springer; 1986, p. 303–54.
[2] Vogt Helmut. Gas-evolving electrodes. In: Comprehensive treatise of electrochemistry. Springer; 1983, p. 445–89.
[3] Vogt H. Chapter 7: Gas-evolving electrodes. In: Comprehensive treatise of electrochemistry, vol. 1, Springer; 1980, p. 445–83.
[4] Wuthrich Rolf, Ziki Jana D Abou. Chapter 3: Gas-evolving electrodes. In: Micromachining using electrochemical discharge phenomenon: fundamentals and application of spark assisted chemical engraving. William Andrew; 2014, p. 35–62.
[5] Haverkort JW. Electrolysers, fuel cells and batteries: analytical modelling. TU Delft OPEN; 2024.
[6] Roald B, Beck W. The dissolution of magnesium in hydrochloric acid. J Electrochem Soc 1951;98(7):277.
[7] Stephan K, Vogt H. A model for correlating mass transfer data at gas evolving electrodes. Electrochim Acta 1979;24:11–8.
[8] Venczel Jozsef. Ueber den stofftransport an gasentwickelnden elektroden [Ph.D. thesis], ETH Zurich; 1961.
[9] Ibl Von N, Venczel J. Investigation of mass transport at gas-evolving electrodes. Metaloberfläche 1970;24:365–74.
[10] Higbie Ralph. The rate of absorption of a pure gas into a still liquid during short periods of exposure. Trans AIChE 1935;31:365–89.
[11] Janssen LJJ. Behaviour of and mass transfer at gas-evolving electrodes. Electrochim Acta 1989;34:161–9.
[12] Janssen LJJ, Barendrecht EJEA. The effect of electrolytic gas evolution on mass transfer at electrodes. Electrochim Acta 1979;24(6):693–9.
[13] Roušar I, Cezner V. Transfer of mass or heat to an electrode in the region of hydrogen evolution—i theory. Electrochim Acta 1975;20(4):289–93.
[14] Janssen LJJ. Mass transfer at gas evolving electrodes. Electrochim Acta 1978;23(2):81–6.
[15] Janssen LJJ, Hoogland JG. The effect of electrolytically evolved gas bubbles on the thickness of the diffusion layer-ii. Electrochim Acta 1973;18:543–50.
[16] Sedahmed GH, Nirdosh I. Intensification of rate of diffusion controlled reactions in a parallel plate electrochemical reactor stirred by a curtain of electrochemically generated gas bubbles. Chem Eng Technol Ind Chem-Plant Equip-Process Eng-Biotechnol 2007;30(10):1406–11.
[17] Stover Richard L, Tobias Charles W, Denn Morton M. Bubble coalescence dynamics. AIChE J 1997;43(10):2385–92.
[18] Dees Dennis Wayne. Mass transfer at gas evolving surfaces in electrolysis. Berkeley: University of California; 1983.
[19] Fouad MG, Gouda T. Natural convection mass transfer at vertical electrodes. Electrochim Acta 1964;9(8):1071–6.

[20] Masliyah Jacob H, Nguyen T. Free convection mass transfer: Laminar and turbulent. Int J Heat Mass Transfer 1975;18(12):1443–7.
[21] Vogt H. The role of single-phase free convection in mass transfer at gas evolving electrodes—i. Theoretical. Electrochim Acta 1993;38(10):1421–6.
[22] Vogt H. The role of single-phase free convection in mass transfer at gas evolving electrodes—ii. Experimental verification. Electrochim Acta 1993;38(10):1427–31.
[23] Denpo K, Teruta S, Fukunaka Y, Kondo Y. Turbulent natural convection along a vertical electrode. Metall Trans B 1983;14:633–43.
[24] Vogt H. Thermal effect on liquid-phase free convection at gas evolving electrodes. Int J Heat Mass Transfer 1993;36(17):4115–21.
[25] Zuber Novak. Nucleate boiling. The region of isolated bubbles and the similarity with natural convection. Int J Heat Mass Transfer 1963;6(1):53–78.
[26] Ibl N. Note on mass transfer at gas sparged electrodes. Electrochim Acta 1979;24(10):1105–8.
[27] Janssen LJJ. Mass transfer at gas-evolving vertical electrodes. J Appl Electrochem 1987;17(6):1177–89.
[28] Beck TR. A contribution to the theory of electrolytic chlorate formation. J Electrochem Soc 1969;116:1038.
[29] Bendrich G, Seiler W, Vogt H. Experimental investigation of combined mass transfer at gas-evolving electrodes with superposition of electrolyte flow. Int J Heat Mass Transfer 1986;29:1741–5.
[30] Whitney Gina M, Tobias Charles W. Mass-transfer effects of bubble streams rising near vertical electrodes. AIChE J 1988;34:1981–95.
[31] Sutija Davor P, Tobias Charles W. Mass-transport enhancement by rising bubble curtains. J Electrochem Soc 1994;141(10):2599.
[32] Sillen CWMP. The effect of gas bubble evolution on the energy efficiency in water electrolysts. 1983.
[33] Janssen LJJ, Barendrecht E. Mechanism of mass transfer of indicator ions to an oxygen-evolving and a hydrogen-evolving electrode in alkaline solution. Electrochim Acta 1985;30(5):683–94.
[34] Pande Nakul, Mul Guido, Lohse Detlef, Mei Bastian. Correlating the short-time current response of a hydrogen evolving nickel electrode to bubble growth. J Electrochem Soc 2019;166(10):E280.
[35] Raman Akash, Penas Pablo, van der Meer Devaraj, Lohse Detlef, Gardeniers Han, Rivas David Fernández. Potential response of single successive constant-current-driven electrolytic hydrogen bubbles spatially separated from the electrode. Electrochim Acta 2022;425:140691.
[36] Bashkatov Aleksandr, Hossain Syed Sahil, Mutschke Gerd, Yang Xuegeng, Rox Hannes, Weidinger Inez M, Eckert Kerstin. On the growth regimes of hydrogen bubbles at microelectrodes. Phys Chem Chem Phys 2022;24(43):26738–52.
[37] Babich Alexander, Bashkatov Aleksandr, Yang Xuegeng, Mutschke Gerd, Eckert Kerstin. In-situ measurements of temperature field and marangoni convection at hydrogen bubbles using schlieren and ptv techniques. Int J Heat Mass Transfer 2023;215:124466.
[38] Iwata Ryuichi, Zhang Lenan, Lu Zhengmao, Gong Shuai, Du Jianyi, Wang Evelyn N. How coalescing bubbles depart from a wall. Langmuir 2022;38(14):4371–7.
[39] Bashkatov Aleksandr, Park Sunghak, Demirkır Çayan, Wood Jeffery A, Koper Marc TM, Lohse Detlef, et al. Performance enhancement of electrocatalytic hydrogen evolution through coalescence-induced bubble dynamics. J Am Chem Soc 2024.
[40] Chen Juanwen, Guo Liejin, Hu Xiaowei, Cao Zhenshan, Wang Yechun. Dynamics of single bubble departure from tio2 nanorod-array photoelectrode. Electrochim Acta 2018;274:57–66.
[41] Wang Mengsha, Nie Tengfei, She Yonglu, Tao Leqing, Luo Xinyi, Xu Qiang, et al. Study on the behavior of single oxygen bubble regulated by salt concentration in photoelectrochemical water splitting. Int J Hydrog Energy 2023;48(61):23387–401.
[42] Wu Rui, Hu Zhihao, Zhang Haojing, Wang Jinqing, Qin Chaozhong, Zhou Ye. Bubbles in porous electrodes for alkaline water electrolysis. Langmuir 2023;40(1):721–33.
[43] Fernandez Damaris, Maurer Paco, Martine Milena, Coey JMD, Möbius Matthias E. Bubble formation at a gas-evolving microelectrode. Langmuir 2014;30(43):13065–74.
[44] Bashkatov Aleksandr, Hossain Syed Sahil, Yang Xuegeng, Mutschke Gerd, Eckert Kerstin. Oscillating hydrogen bubbles at pt microelectrodes. Phys Rev Lett 2019;123:214503.
[45] Park Sunghak, Liu Luhao, Demirkır Çayan, van der Heijden Onno, Lohse Detlef, Krug Dominik, et al. Solutal marangoni effect determines bubble dynamics during electrocatalytic hydrogen evolution. Nat Chem 2023;15(11):1532–40.
[46] Lu Xinlong, Yadav Devendra, Ma Benchi, Ma Lijing, Jing Dengwei. Rapid detachment of hydrogen bubbles for electrolytic water splitting driven by combined effects of marangoni force and the electrostatic repulsion. J Power Sources 2024;599:234217.
[47] Bashkatov Aleksandr, Babich Alexander, Hossain Syed Sahil, Yang Xuegeng, Mutschke Gerd, Eckert Kerstin. H2 bubble motion reversals during water electrolysis. J Fluid Mech 2023;958:A43.
[48] Ibl N, Adam E, Venczel J, Schalch E. Stofftransport bei der elektrolyse mit gasrührung. Chem Ing Tech 1971;43(4):202–15.
[49] Ibl N, Kind R, Adam E. Mass transfer at electrodes with gas stirring. An Quim 1975.
[50] Vondrak J, Balej J. Influence of mercury on hydrogen overvoltage on solid metal electrodes—i. Stationary polarization curves of hydrogen deposition on pure and poisoned electrodes. Electrochim Acta 1970;15(10):1653–65.
[51] Fouad MG, Sedahmed GH. Effect of gas evolution on the rate of mass transfer at vertical electrodes. Electrochim Acta 1972;17(4):665–72.
[52] Fouad MG, Sedahmed GH. Mass transfer at horizontal gas-evolving electrodes. Electrochim Acta 1973;18(1):55–8.
[53] Janssen LJJ, Barendrecht E. The effect of electrolytic gas evolution on mass transfer at electrodes. Electrochim Acta 1979;24(6):693–9.
[54] Janssen LJJ, Hoogland JG. The effect of electrolytically evolved gas bubbles on the thickness of the diffusion layer. Electrochim Acta 1970;15(6):1013–23.
[55] Green Mino, Robinson Paul H. Kinetics of the cathodic reduction of anions: Germanium oxides. J Electrochem Soc 1959;106(3):253.
[56] Hiraoka S, Yamada I, Mori H, Sugimoto H, Hakushi N, Matsuura A, et al. Mass transfer and shear stress on a vertical electrode with gas evolution. Electrochim Acta 1986;31(3):349–54.
[57] Kind Richard. Untersuchung des Stofftransports und der Rührwirkung bei gasentwickelnden Elektroden [Ph.D. thesis], ETH Zurich; 1975.
[58] Fukunaka Y, Suzuki K, Ueda A, Kondo Y. Mass-transfer rate on a plane vertical cathode with hydrogen gas evolution. J Electrochem Soc 1989;136:1002–9.
[59] Alkire Richard, Lu Po-Yen. Effect of hydrogen evolution on current distribution during electrodeposition at vertical electrodes. J Electrochem Soc 1979;126(12):2118.
[60] Chen SF, O'Keefe TJ. Enhanced mass transport in electrogalvanizing systems by hydrogen evolution. Electrochim Acta 1988;33(6):789–94.
[61] Vogt Helmut. The rate of gas evolution of electrodes—i. An estimate of the efficiency of gas evolution from the supersaturation of electrolyte adjacent to a gas-evolving electrode. Electrochim Acta 1984;29(2):167–73.
[62] Joe JMChin Kwie, Janssen LJJ, Van Strelen SJD, Verbunt JHG, Sluyter WM. Bubble parameters and efficiency of gas bubble evolution for a chlorine-, a hydrogen-and an oxygen-evolving wire electrode. Electrochim Acta 1988;33(6):769–79.
[63] Janssen LJJ, Hoogland JG. The effect of electrolytically evolved gas bubbles on the thickness of the diffusion layer—ii. Electrochim Acta 1973;18(8):543–50.
[64] Nicolai H, Herzhaft B, Hinch EJ, Oger L, Guazzelli E. Particle velocity fluctuations and hydrodynamic self-diffusion of sedimenting non-brownian spheres. Phys Fluids 1995;7(1):12–23.
[65] Fouad MG, Sedahmed GH. Effect of gas evolution on the rate of mass transfer at vertical electrodes. Electrochim Acta 1972;17(4):665–72.
[66] Hiraoka S, Yamada I, Mori H, Sugimoto H, Hakushi N, Matsuura A, et al. Mass transfer and shear stress on a vertical electrode with gas evolution. Electrochim Acta 1986;31:349–54.
[67] Valle N, Haverkort JW. Analytical mass transfer coefficients for natural convection from vertical gas-evolving electrodes. Int J Heat Mass Transfer 2024;225:125390.
[68] Ostrach Simon. An analysis of laminar free-convection flow and heat transfer about a flat plate parallel to the direction of the generating body force. 1953.
[69] Sparrow EM, Gregg JL. Laminar free convection from a vertical plate with uniform surface heat flux. J Fluids Eng 1956;78(2):435–40.
[70] Sparrow EM, Eichhorn R, Gregg JL. Combined forced and free convection in a boundary layer flow. Phys Fluids 1959;2:319–28.
[71] Janssen LJJ, Stralen SJD Van. Bubble behaviour on and mass transfer to an oxygen-evolving transparent nickel electrode in alkaline solution. Electrochim Acta 1981;26(8):1011–22.
[72] Balzer RJ, Vogt H. Effect of electrolyte flow on the bubble coverage of vertical gas-evolving electrodes. J Electrochem Soc 2003;150(1):E11.
[73] Nefedov VG. Mass transfer to a gas-generating electrode. Russ J Electrochem 1998;34(1):16–24.
[74] White Malcolm L. The wetting of gold surfaces by water1. J Phys Chem 1964;68(10):3083–5.
[75] Hong Kwang Taek, Imadojemu Harris, Webb RL. Effects of oxidation and surface roughness on contact angle. Exp Therm Fluid Sci 1994;8(4):279–85.
[76] Janssen LJJ, Sillen CWMP, Barendrecht E, van Stralen SJD. Bubble behaviour during oxygen and hydrogen evolution at transparent electrodes in koh solution. Electrochim Acta 1984;29:633–42.
[77] Matsushima Hisayoshi, Iida Takami, Fukunaka Yasuhiro. Gas bubble evolution on transparent electrode during water electrolysis in a magnetic field. Electrochim Acta 2013;100:261–4.
[78] Marcus Yizhak. Surface tension of aqueous electrolytes and ions. J Chem Eng Data 2010;55(9):3641–4.
[79] Coehn Alfred, Neumann Hans. Elektrostatische erscheinungen an elektrolytisch entwickelten gasblasen: I. elektrostatische anziehung und blasengröße. Z Phys 1923;20:54–67.
[80] Brandon NP, Kelsall GH, Levine S, Smith AL. Interfacial electrical properties of electrogenerated bubbles. J Appl Electrochem 1985;15:485–93.
[81] Kabanow B, Frumkin A. Über die grösse elektrolytisch entwickelter gasblasen. Z Phys Chem 1933;165(1):433–52.

[82] Möller Hans Georg. Elektrolytische vorgänge an der elektrodenoberfläche. überspannung und elektrokapillarität. Z Phys Chem 1909;65(1):226–54.
[83] Alam Raquibul, Shang Julie Q, Khan Adnan Hossain. Bubble size distribution in a laboratory-scale electroflotation study. Environ Monit Assess 2017;189:1–14.
[84] da Cruz Samantha Grisol, Dutra Achilles JB, Monte Marisa BM. The influence of some parameters on bubble average diameter in an electroflotation cell by laser diffraction method. J Environ Chem Eng 2016;4(3):3681–7.
[85] Glas JP, Westwater JW. Measurements of the growth of electrolytic bubbles. Int J Heat Mass Transfer 1964;7(12):1427–43.
[86] Campanella Luigi. Zero charge potential of metals. J Electroanal Chem Interfacial Electrochem 1970;28(1):228–32.
[87] Sides Paul J, Tobias Charles W. A close view of gas evolution from the back side of a transparent electrode. J Electrochem Soc 1985;132(3):583.
[88] Putt Ronald Alan. Studies of the events occurring at gas-evolving electrodes. Technical report, Lawrence Berkeley National Laboratory; 1975.
[89] Lv Pengyu, Peñas Pablo, The Hai Le, Eijkel Jan, van den Berg Albert, Zhang Xuehua, et al. Self-propelled detachment upon coalescence of surface bubbles. Phys Rev Lett 2021;127(23):235501.
[90] Westerheide DE, Westwater JW. Isothermal growth of hydrogen bubbles during electrolysis. AIChE J 1961;7:357–62.
[91] Janssen LJJ, Hoogland JG. The effect of electrolytically evolved gas bubbles on the thickness of the diffusion layer. Electrochim Acta 1970;15(6):1013–23.
[92] Han Yifan, Bashkatov Aleksandr, Huang Mengyuan, Eckert Kerstin, Mutschke Gerd. Impact of tracer particles on the electrolytic growth of hydrogen bubbles. Phys Fluids 2024;36(1).
[93] Hashemi SMohammad H, Karnakov Petr, Hadikhani Pooria, Chinello Enrico, Litvinov Sergey, Moser Christophe, et al. A versatile and membrane-less electrochemical reactor for the electrolysis of water and brine. Energy Environ Sci 2019;12(5):1592–604.
[94] Lubetkin Steven. The motion of electrolytic gas bubbles near electrodes. Electrochim Acta 2002;48(4):357–75.
[95] Yang Xuegeng, Baczyzmalski Dominik, Cierpka Christian, Mutschke Gerd, Eckert Kerstin. Marangoni convection at electrogenerated hydrogen bubbles. Phys Chem Chem Phys 2018;20(17):11542–8.
[96] Guelcher Scott A, Solomentsev Yuri E, Anderson John L, Boehmer Marcel, Sides Paul J. The effect of surface induced flows on bubble and particle aggregation. In: Proceedings of the fourth microgravity fluid physics and transport phenomena conference. 1999.
[97] Lu Xinlong, Nie Tengfei, Li Xiaoping, Jing Li, Zhang Yiming, Ma Lijing, et al. Insight into ph-controlled bubble dynamics on a pt electrode during electrochemical water splitting. Phys Fluids 2023;35(10).
[98] Quinn Anthony, Sedev Rossen, Ralston John. Contact angle saturation in electrowetting. J Phys Chem B 2005;109(13):6268–75.
[99] Taherian Fereshte, Leroy Frédéric, Heim Lars-Oliver, Bonaccurso Elmar, van der Vegt Nico FA. Mechanism for asymmetric nanoscale electrowetting of an ionic liquid on graphene. Langmuir 2016;32(1):140–50.
[100] Jiang Chen, Ma Hanbin, Hasko David G, Nathan Arokia. Influence of polarization on contact angle saturation during electrowetting. Appl Phys Lett 2016;109(21).
[101] Guo Yuanyuan, Deng Yong, Xu Bojian, Henzen Alex, Hayes Rob, Tang Biao, et al. Asymmetrical electrowetting on dielectrics induced by charge transfer through an oil/water interface. Langmuir 2018;34(40):11943–51.
[102] Sarma Satirtha K, Singh Aditya, Mohan Ratan, Shukla Anupam. Computational fluid dynamics simulation of bubble hydrodynamics in water splitting: Effect of electrolyte inflow velocity and electrode morphology on cell performance. Int J Hydrog Energy 2023;48(47):17769–82.
[103] Egan EW, Tobias CW. Measurement of interfacial re-equilibration during hydrogen bubble coalescence. J Electrochem Soc 1994;141(5):1118.
[104] Janssen LJJ. Behaviour of and mass transfer at gas-evolving electrodes. Electrochim Acta 1989;34(2):161–9.
[105] Corcione Massimo. Heat transfer correlations for free convection from upward-facing horizontal rectangular surfaces. WSEAS Trans Heat Mass Transf 2007;2(3):48–60.
[106] Kitamura Kenzo, Kimura Fumiyoshi. Heat transfer and fluid flow of natural convection adjacent to upward-facing horizontal plates. Int J Heat Mass Transfer 1995;38(17):3149–59.
[107] Vliet Gary C. Natural convection local heat transfer on constant-heat-flux inclined surfaces. J Heat Transf 1969;91(4):511–6.
[108] Vliet GC, Ross DC. Turbulent natural convection on upward and downward facing inclined constant heat flux surfaces. J Heat Transf. 1975;94(4):549–54.
[109] Haverkort JW. Modeling and experiments of binary electrolytes in the presence of diffusion, migration, and electro-osmotic flow. Phys Rev A 2020;14(4):044047.
[110] Young NO, Goldstein Jo S, Block MJ0087. The motion of bubbles in a vertical temperature gradient. J Fluid Mech 1959;6(3):350–6.
[111] Brennen Christopher E. Cavitation and bubble dynamics. Cambridge University Press; 2014.
[112] Badiali Jean P, Goodisman Jerry. Lippmann equation and the ideally polarizable electrode. J Phys Chem 1975;79(3):223–32.